Supporting Information

Unveiling the Multifunctional Properties of Dicyanoisophorone Derivatives: From White OLEDs and Picric Acid Sensing to Nonlinear Optics

Khushdeep Kaur, [a] Oleksandr Bezvikonnyi, [a,b] Dmytro Volyniuk, [a] Weizhen Liu, [c] Yovan de Coene, [c] Koen Clays, *[c] Kamaljit Singh, [d] Ehsan Ullah Rashid, [a] Asta Dabuliene, [a] Oleksandr Navozenko, [e] and Juozas V. Grazulevicius*[a]

[a]Department of Polymer Chemistry and Technology, Faculty of Chemical Technology, Kaunas University of Technology, K. Baršausko st. 59, LT-51423 Kaunas, Lithuania.

[b]Institute of Solid-State Physics, University of Latvia, Kengaraga 8, LV-1063, Riga, Latvia.

[c]Department of Chemistry, University of Leuven, Celestijnenlaan 200D, B-3001 Leuven, Belgium.

[d]Department of Chemistry, UGC Centre of Advanced Study, Guru Nanak Dev University, Amritsar 143005, India.

[e]Department of Experimental Physics, Faculty of Physics, Taras Shevchenko National University of Kyiv, Akademika Glushkova Av. 4, 03127, Kyiv, Ukraine.

* Corresponding authors. E-mail: juozas.grazulevicius@ktu.lt, Koen.Clays@kuleuven.be.

Content **Pages**

S1. Instrumentation

Avantes AvaSpec-2048XL spectrometer was used for the measurements of absorption and EL spectra. Edinburgh Instruments FLS 980 spectrometer was used for the measurements of emission spectra and quantum yields by an absolute method using an integrating sphere. PicoQuant PDL 820 ps diode laser was used for the measurements of emission decay curves via time-correlated single photon counting technique. Malvern Mastersizer 3000 laser diffraction particle size analyzer was used for the studies of aggregatres.

Drift charge transport characteristics of the investigated materials were investigated using the TOF and CELIV techniques. For the TOF and CELIV measurements, films were made by thermal vacuum deposition. An EKSPLA NL300 laser (excitation wavelength of 355 nm), a 6517B electrometer (Keithley), and a TDS 3032C oscilloscope (Tektronix) were used in TOF and CELIV setups.

The density functional theory (DFT) was utilized for the computational studies of the compounds (B3LYP functional combined with the 6–31G(d,p) basis set) using the Gaussian software package.[1] To simulate the absorption spectra, the lowest 30 vertical electronic transitions were calculated using the time-dependent DFT (TDDFT) method combined with the polarizable continuum model (PCM) to account for solvent effects. Molecular orbitals were visualized by using Gaussview. Theoretical first hyperpolarizability values were calculated at CAM-B3LYP functional combined with the 6–31G(d,p) basis set. Natural bond orbitals (NBO) analysis, and Mulliken charges using DFT/B3LYP method with 6-31G (d, p) basis set in gaseous phase (isosurface value 0.00[2]).

Kurt J. Lesker equipment built in the MBRAUN EcoVap4G glove box was used for the fabrication of OLEDs and preparation of samples for TOF measurements via thermal vacuum evaporation technique. The deposition of organic layer was done with a rate of 1-2 Angstroms per s under the pressure of pressure was $2 \cdot 10^{-6}$ mbar. The samples were not passivated. Keithley 2400C sourcemeter, PH100-Si-HA-D0 calibrated photodiode, 11S-LINK PC-based power and energy monitor were used for the simultaneous measurements of the current density-voltage and luminance-voltage dependences.

1,4,5,8,9,11-Hexaazatriphenylenehexacarbonitrile (HAT-CN) and LiF were selected for the deposition of hole and electron injection layers, respectively. 4,4',4"-Tris(carbazol-9-

yl)triphenylamine (TCTA) and 2,2',2"-(1,3,5-Benzinetriyl)-tris(1-phenyl-1-H-benzimidazole) (TPBi) were chosen for the deposition of hole and electron transport layers, respectively. Diphenyl[4-(triphenylsilyl)phenyl]phosphine oxide (TSPO1) was employed for the deposition of hole blocking layer. 1,3-Di(9H-carbazol-9-yl)benzene (mCP) was taken as a host material for K2.

For Hyper-Rayleigh scattering measurements, a custom designed optical setup was used to determine the first hyperpolarizabilities of the compounds. The laser (Insight DS+, Spectra-Physics) allows for a tunable output between 680 and 1300 nm. The former delivers femtosecond (~120 fs) pulses at an 80 MHz repetition rate. The output beam ($1/e^2 < 1.2$ mm) has a Gaussian profile ($M^2 < 1.1$) is horizontally polarized (the plane of the optical table). A combination of an achromatic half-wave plate and Glan-Laser polarizer allows controlling the output power in accordance to Malus's law. The polarizer is placed in such a way that the extraordinary ray is vertically polarized. The average power which is sent into the sample typically ranges from 500 to 1000 mW. The beam is routed to the input lens (aspheric, f = 8.00 mm) by a series of mirrors. A long pass filter with a cut-off at 690 nm is used to prevent any higher harmonic generation from the laser or the optics from entering the sample. The quartz cuvette (10 × 4 mm) is placed in a custom translation mount, which allows defining the path length of the focal point relative to the side walls. Light is collected at 90° by an achromatic, aspheric condenser lens (f = 30 mm). The collimated beam passes a series of three large broadband dielectric elliptical mirrors to rotate the image 90°. The latter ensures maximal resolution of the spectrograph (vertically oriented slit). The collimated beam is focused on the spectrograph (IS/SM 500, Bruker) with a plano-convex lens, matching the focal length of the spectrograph (f = 200 mm, f/8). A blocking edge filter (FF01-720/SP-25, Semrock) ensures high optical density in the laser excitation range. One of two gratings (50 grooves/mm, 600 nm blaze or 150 grooves/mm, 500 nm blaze) were used, depending on the desired resolution, diffraction range and spectral profile of multiphoton emission spectra. An EMCCD camera (Ixon Ultra 897, Andor Solis) was used to image the spectra.

Due to the trade-off between resonance enhancement and self-absorption at the second-harmonic wavelength. A concentration series (different concentrations + solvent) was made *in situ* with the different dilution factors to give a broad range (*vide infra Fig.S34-S41*). Multiple spectra were

recorded for each concentration. These spectra were corrected for multiphoton fluorescence (MPF) using a polynomial function. The 'fluorescence-free' spectrum was then fitted to a Gaussian function. Since each concentration was measured multiple times, the standard deviation on the Gaussian areas was taken as the error (equation 1).

$$\sigma = \sqrt{\frac{\sum_{i=1}^{n}(y_i - \bar{y})^2}{n}} \quad \text{……..(1)}$$

$$w_i = \frac{1}{\sigma^2} \text{ ……..(2)} \qquad \sigma_{slope} = \frac{\sqrt{S2e}}{\sqrt{SSx}} \text{ …..(3)} \qquad S2e = \frac{(CCx - CCy)^2}{n} \text{…….(4)}$$

$$SSx = \sum_{i=1}^{n}(C_i - \overline{C})^2 \text{……..(5)} \quad \sigma_{intercept} = \sigma_{slope}\sqrt{\frac{X2i}{n}} \text{ ……(6)} \quad X2i = \sum_{i=1}^{n} C_i \text{….(7)}$$

Next, $I_{2\omega}$ normalized for the integration time were plotted as a function of the concentration. By performing a linear regression through the data points, a slope and intercept was obtained, with the intercept the HRS intensity of the solvent. For the error calculation we use a weighted fit where the weight of each data point is given by equation 2, while the standard error of the slope is given by equation 3 and 4. Where CC_x is the measured intensity and CC_y is the one extracted from the linear regression. In equation 5, C is the concentration and the standard error for the intercept is given by equation 6, where $X2i$ is given by equation 7.

The hyperpolarizabilities were calculated using the internal reference method. For a two-component system, where solvent and solute both contribute to the HRS intensity, the intensity $I_{2\omega}$ is given by equation 8.

$$I_{2\omega} = G(N_s < \beta_{HRS}^2 >_s + N_x < \beta_{HRS}^2 >_x) I_\omega^2 \quad \text{….(8)}$$

where N_s and N_x are the number densities of the solvent and the solute respectively. The unknown hyperpolarizability of the solute ($<\beta^2_{HRS}>_x$) can be calculated if that of the solvent ($<\beta^2_{HRS}>_s$) was known. By measuring $I_{2\omega}$ as a function of concentration, $<\beta_{HRS}>_x$ can be

extracted by rewriting equation 9. By taking GN_s ($<\beta^2_{HRS}>_s$) as the intercept of the latter linear concentration dependence towards $I_{2\omega}$, and G ($<\beta^2_{HRS}>_x$) as the slope, results in equation 10.

$$< \beta_{HRS} >_x = < \beta_{HRS} >_s \sqrt{\frac{slope}{intercept} N_s} \quad \ldots\ldots(9)$$

For determining the error in $<\beta_{HRS}>_x$, standard error propagation rules were applied using equation 10.

$$\sigma(\beta_{HRS} >_x) = \beta_{HRS} >_s \sqrt{N_s} \sqrt{\frac{1}{4 \frac{slope}{intercept}}} \sqrt{\left(\frac{1}{intercept}\right)^2 \sigma_{slope}^2 + \left(-\frac{slope}{intercept^2}\right)^2 \sigma_{intercept}^2} \ldots(10)$$

S2. Synthetic procedures

Synthesis of intermediates

2-(3,5,5-trimethylcyclohex-2-en-1-ylidene)malononitrile (**ISP)** was synthesized according to the procedure mentioned in literature.[44]

*Synthesis of (E)-2-(3-(4-bromostyryl)-5,5-dimethylcyclohex-2-en-1-ylidene)malononitrile (**Br-Ph-ISP**):*

A solution of 4-bromobenzaldehyde (Br-BA) (1eq, 0.200g, 1.08mmol) and ISP (1.5 eq, 0.302g, 1.62mmol) in 20 ml ethanol is cooled and stirred to 0^0C in 50ml round bottom flask followed by the addition of catalytic amount of piperidine. The reaction mixture is further stirred at room temperature for 30 mins followed by heating at 60-70^0C for 8h. After completion (TLC), reaction mixture was cooled and yellow precipitates were filtered. Recrystallisation of crude precipitates in isopropanol furnished the yellow solid (0.313g, 82% yield). $\mathbf{R_f}$: 0.48 (ethyl acetate: hexane 1:20, v/v). mp: 195-200 ^{0}C. **^{1}H NMR** (400 MHz, $CDCl_3$), δ (ppm): 1.01 (s, 6H), 2.39 (s, 2H), 2.54 (s, 2H), 6.79 (s, 1H), 6.90 (s, 2H), 7.30 (d, J=7.9 Hz, 2H), 7.46 (d, J= 8.0 Hz, 2H). **^{13}C NMR** (101 MHz, $CDCl_3$), δ (ppm): 28.0, 32.1, 39.2, 43.0, 79.3, 112.6, 113.4, 123.9, 124.0, 128.9, 129.8, 132.3, 134.6, 135.5, 153.3, 169.1. **MS** (ESI+): Calculated for $C_{19}H_{17}N_2$ Br = 352.06; Obtained = 352.88 $[M]^+$

General procedure for the synthesis of K1-K6 using Suzuki cross coupling reaction

Br-Ph-ISP (1.0 eq.) and respective boronic acid (1.5-2.3 eq.) was dissolved in degassed toluene (15-20ml) in a dry Schlenk flask at room temperature under inert conditions. The reaction mixture was further degassed and stirred for 30 mins followed by the addition of catalytic amount of Pd $(PPh_3)_4$. After addition of degassed solution of 2M K_2CO_3 (2-4eq.), the reaction mixture was subjected to heating until completion of reaction (TLC). After cooling, extractive workup was performed using ethyl acetate (2×50 ml). The organic extract was dried using anhydrous sodium sulphate (15.90, 150mmol) and filtered. After removal of the solvent under reduced pressure, final products were obtained which were purified using column chromatography (hexane/ethyl acetate or THF as eluent) and further washed with isopropanol.

*Synthesis of (E)-2-(5,5-dimethyl-3-(4-(9-phenyl-9H-carbazol-2-yl)styryl)cyclohex-2-en-1-ylidene)malononitrile (**K1**):*

K1 was prepared using general procedure (described above) from 1.5 eq of (9-phenyl-9*H*-carbazol-2-yl)boronic acid (0.245 g, 0.85 mmol), 1eq of Br-Ph-ISP (0.200g, 0.57mmol), 2eq of 2M K_2CO_3 solution and catalytic amount of $Pd(PPh_3)_4$ (0.05 eq) at 110^0C. Purification of product was achieved using column chromatography using ethyl acetate: hexane (1:13 v/v) as eluent. The final product was obtained as orange powder (0.120g, 41% yield, FW=515.66 $gmol^{-1}$), R_f: 0.32 (ethyl acetate: hexane 1:6, v/v), m.p.= 298^0C (measured from DSC). **ATR-IR** (solid state on ATR, $\boldsymbol{\nu_{max}}$, cm^{-1}): 3027 (aromatic C–H), 2945 (alkyl C–H), 2209 (nitrile C≡N), 1602 (alkene C=C stretch), 1556 (alkyl C-H bending), 1227 (C-N), 954 (trans alkene C=C bending). **^{1}H NMR** (400 MHz, $CDCl_3$), δ (ppm): 1.09 (s, 6H), 2.49 (s, 2H), 2.61 (s, 2H), 6.89 (s, 1H), 6.99-7.11 (q, J=16Hz, 2H), 7.31 (t, J=12Hz ,1H), 7.39-7.45 (m, 2H), 7.49-7.70 (m,11H), 8.15-8.22 (q, J=8Hz, 2H). **^{13}C NMR** (101 MHz, $CDCl_3$), δ (ppm): 28.1, 32.1, 39.3, 43.0, 78.6, 108.1, 109.9, 119.4, 120.2, 120.4, 120.8, 123.0, 123.1, 123.6, 126.3, 127.3, 127.7, 128.0, 128.9, 129.8, 130.1, 134.4, 136.7, 137.5, 138.2, 139.5, 141.5, 141.6, 143.3, 153.9, 169.2. **MS** (ESI-): Calculated for $C_{37}H_{29}N_3$ =515.24; Obtained = 513.78 $[M-2H]^+$

*Synthesis of (E)-2-(3-(4-(9H-fluoren-2-yl)styryl)-5,5-dimethylcyclohex-2-en-1-ylidene)malononitrile (**K2**):*

K2 was prepared using general procedure (described above) from 1.5 eq of (9H-fluoren-2-yl)boronic acid (0.178g, 0.85 mmol), 1eq of Br-Ph-ISP (0.200g, 0.57mmol), 2eq of 2M K_2CO_3 solution and catalytic amount of $Pd(PPh_3)_4$ at 110^0C. The final product was obtained as light orange powder (0.169g, 68% yield, FW=438.57 $gmol^{-1}$), R_f : 0.51 (ethyl acetate: hexane 1:4, v/v), m.p.= 280^0C (measured from DSC). Purification of product was achieved using column chromatography using ethyl acetate: hexane (1:9 v/v) as eluent. **ATR-IR** (solid state on ATR, $\boldsymbol{\nu_{max}}$, cm^{-1}): 3038 (aromatic C–H), 2952 (alkyl C–H), 2208 (nitrile C≡N), 1610 (alkene C=C stretch), 1552 (alkyl C-H bending), 966 (trans alkene C=C bending).**^{1}H NMR** (400 MHz, $CDCl_3$), δ (ppm): 1.10 (s, 6H), 2.50 (s, 2H), 2.61 (s, 2H), 3.97 (s, 2H), 6.87 (s, 1H), 7.02-7.13 (q, J=16Hz, 2H), 7.33 (t, J=7.4Hz, 1H), 7.41 (t, J=7.4Hz, 1H), 7.56-7.87 (m, 9H). **^{13}C NMR** (101 MHz, $CDCl_3$), δ (ppm): 28.1, 32.1, 37.0, 39.3, 43.0, 78.6, 112.7, 112.8, 113.6, 120.1, 120.3, 123.6, 125.1, 125.7, 126.9, 127.0, 127.6, 128.1, 128.9, 134.5, 136.7, 138.6, 141.2, 141.6, 142.8, 143.5, 144.1, 153.9, 169.2. **MS** (ESI-): Calculated for $C_{32}H_{26}N_2$ =438.21; Obtained = 437.10$[M-H]^+$

*Synthesis of (E)-2-(5,5-dimethyl-3-(4-(phenanthren-9-yl)styryl)cyclohex-2-en-1-ylidene)malononitrile (**K5**):*

K5 was prepared using general procedure (described above) from 1.5 eq of phenanthren-9-ylboronic acid (0.189 g, 0.85 mmol), 1eq of Br-Ph-ISP (0.200g, 0.57mmol), 2eq of 2M K_2CO_3 solution and catalytic amount of $Pd(PPh_3)_4$ at 110^0C. The final product was obtained as bright yellow powder (0.130g, 51% yield, FW=450.59 $gmol^{-1}$), R_f: 0.50 (THF: hexane 1:5, v/v), m.p.= 203^0C (measured from DSC). Purification of product was achieved using column chromatography using THF: hexane (1:9 v/v) as eluent. **ATR-IR** (solid state on ATR, $\boldsymbol{\nu_{max}}$, cm^{-1}): 3036 (aromatic C–H), 2959 (alkyl C–H), 2216 (nitrile C≡N), 1608 (alkene C=C stretch), 1560 (alkyl C-H bending), 961 (trans alkene C=C bending).**^{1}H NMR** (400 MHz, $CDCl_3$), δ (ppm): 1.11 (s, 6H), 2.52 (s, 2H), 2.63 (s, 2H), 6.89 (s, 1H), 7.07-7.19 (q, J= 16.1Hz, 2H), 7.51-7.72 (m, 9H), 7.91 (m, 2H), 8.73 (d, J= 8.2Hz, 1H), 8.79 (d, J= 8.3Hz, 1H). **^{13}C NMR** (101 MHz, $CDCl_3$), δ (ppm): 28.1, 32.1, 39.3, 43.0, 78.8, 112.8, 113.5, 122.6, 123.1, 123.7, 126.7, 126.9, 127.0, 127.6, 128.8, 129.3, 130.1, 130.7, 130.8, 131.4, 134.8, 136.7, 137.9, 142.5, 153.8, 169.3. **MS** (ESI+): Calculated for $C_{33}H_{26}N_2$ =450.21; Obtained = 448.56 $[M-2H]^+$

*Synthesis of (E)-2-(3-(4-(9,9-dimethyl-9H-fluoren-2-yl)styryl)-5,5-dimethylcyclohex-2-en-1-ylidene)malononitrile (**K6**):*

K6 was prepared using general procedure (described above) from 1.5 eq of (9,9-dimethyl-9H-fluoren-2-yl)boronic acid (0.245 g, 0.85 mmol), 1eq of Br-Ph-ISP (0.200g, 0.57mmol), 2eq of 2M K_2CO_3 solution and catalytic amount of $Pd(PPh_3)_4$ at 110^0C. The final product was obtained as orange powder (0.190g, 72% yield, FW= 466.63 $gmol^{-1}$), R_f: 0.39 (THF: hexane 1:7, v/v), m.p.= 227^0C (measured from DSC). Purification of product was achieved using column chromatography using THF: hexane (1:14 v/v) as eluent. **ATR-IR** (solid state on ATR, $\boldsymbol{\nu_{max}}$, cm^{-1}): 3024 (aromatic C–H), 2922 (alkyl C–H), 2213 (nitrile C≡N), 1609 (alkene C=C stretch), 1557 (alkyl C-H bending), 963 (trans alkene C=C bending).**^{1}H NMR** (400 MHz, $CDCl_3$), δ (ppm): 1.03 (s, 6H), 1.47 (s, 6H), 2.43 (s, 2H), 2.55 (s, 2H), 6.81 (s, 1H), 6.95-7.07 (q, J=16.1Hz, 2H), 7.25-7.31 (m, 2H), 7.39 (d, J= 6.6Hz, 1H), 7.54 (d, J=7.7Hz, 3H), 7.63-7.73 (m, 5H). **^{13}C NMR** (101 MHz, $CDCl_3$), δ (ppm): 27.2, 28.1, 32.1, 39.3, 43.0, 78.6, 112.8, 113.6, 120.2, 120.5, 121.2, 122.7, 123.6, 126.1, 127.1, 127.5, 128.1, 128.9, 134.5, 136.7, 138.7, 139.1, 139.2, 142.9, 153.8, 153.9, 154.4 169.3. **MS** (ESI-): Calculated for $C_{34}H_{30}N_2$ = 466.24; Obtained = 465.31$[M-H]^+$

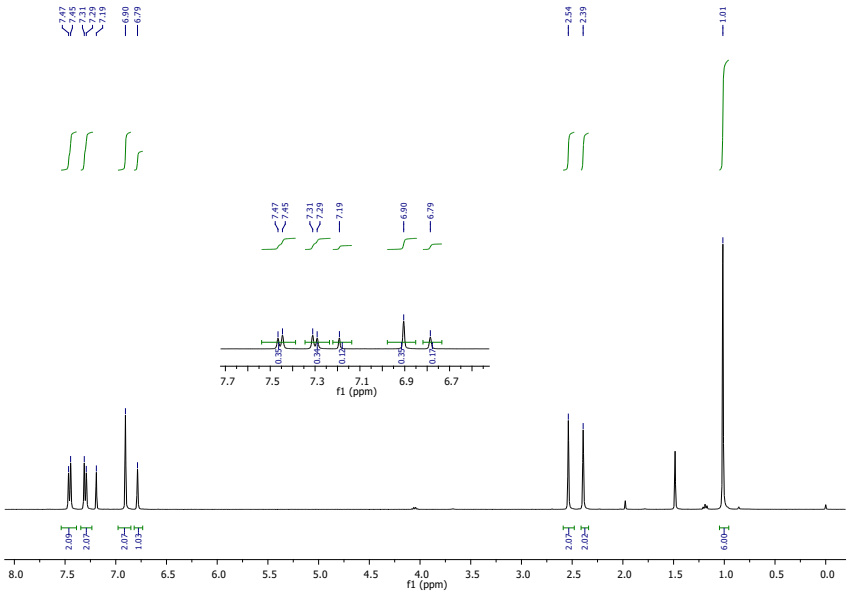

Figure S1. ^{1}H NMR spectrum of Br-Ph-ISP (400MHz, $CDCl_3$).

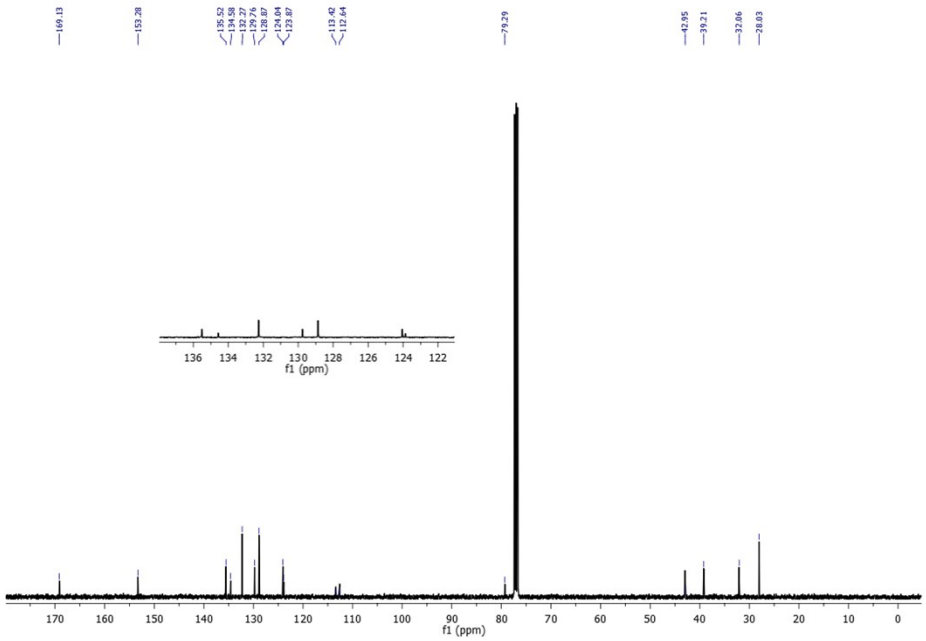

Figure S2. ^{13}C NMR spectrum of Br-Ph-ISP (101MHz, $CDCl_3$).

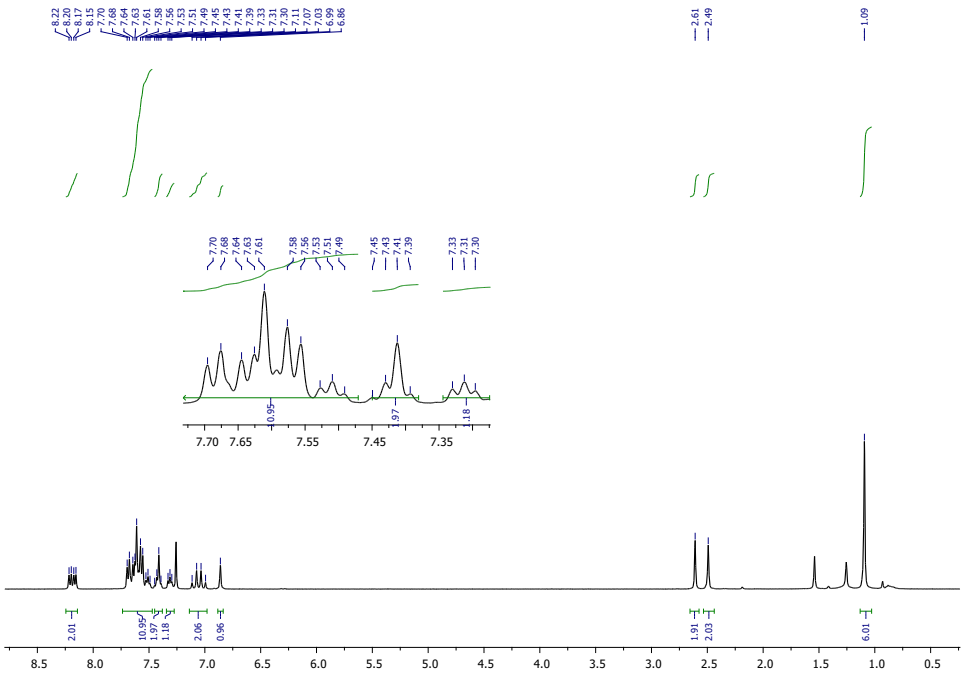

Figure S3. ^{1}H NMR spectrum of K1 (400MHz, $CDCl_3$).

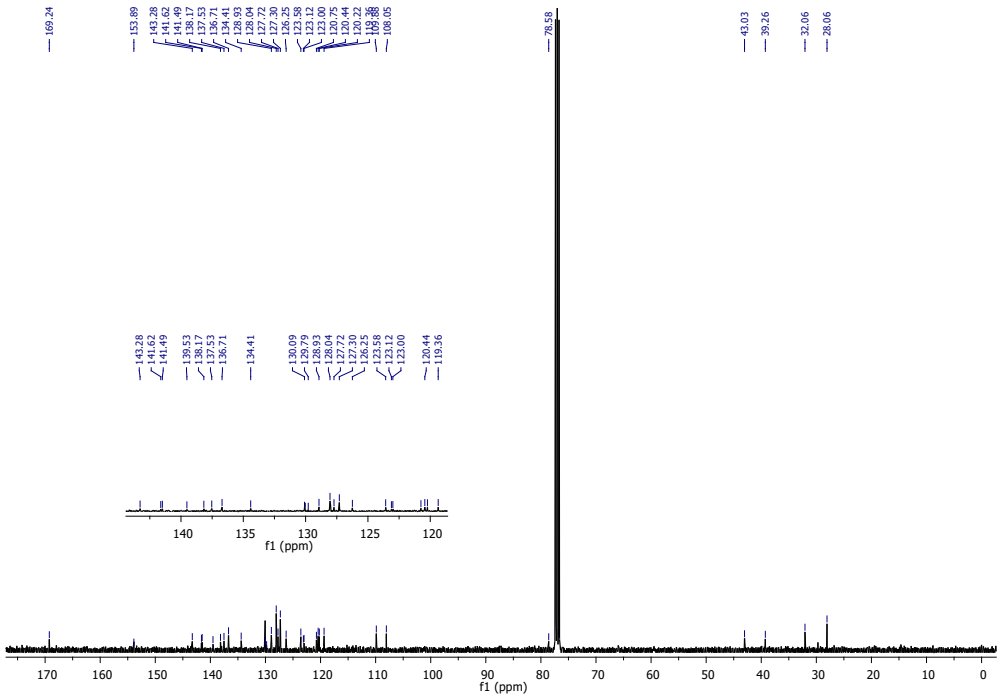

Figure S4. ^{13}C NMR spectrum of K1 (101 MHz, $CDCl_3$).

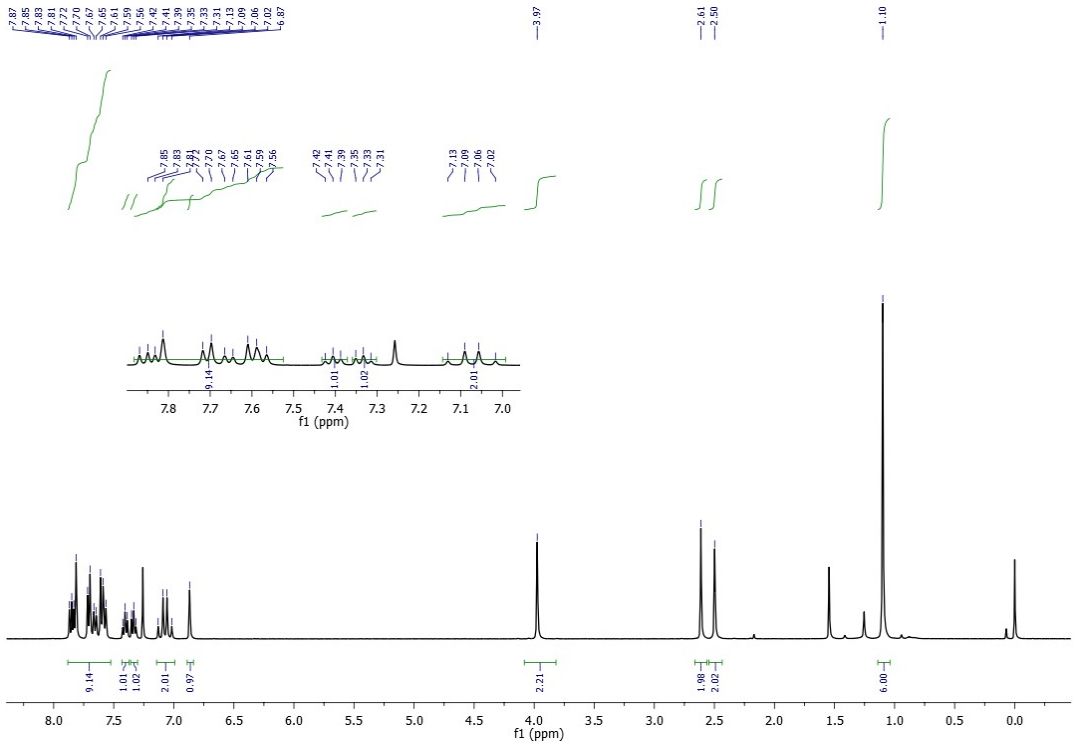

Figure S5. ^{1}H NMR spectrum of K2 (400MHz, $CDCl_3$).

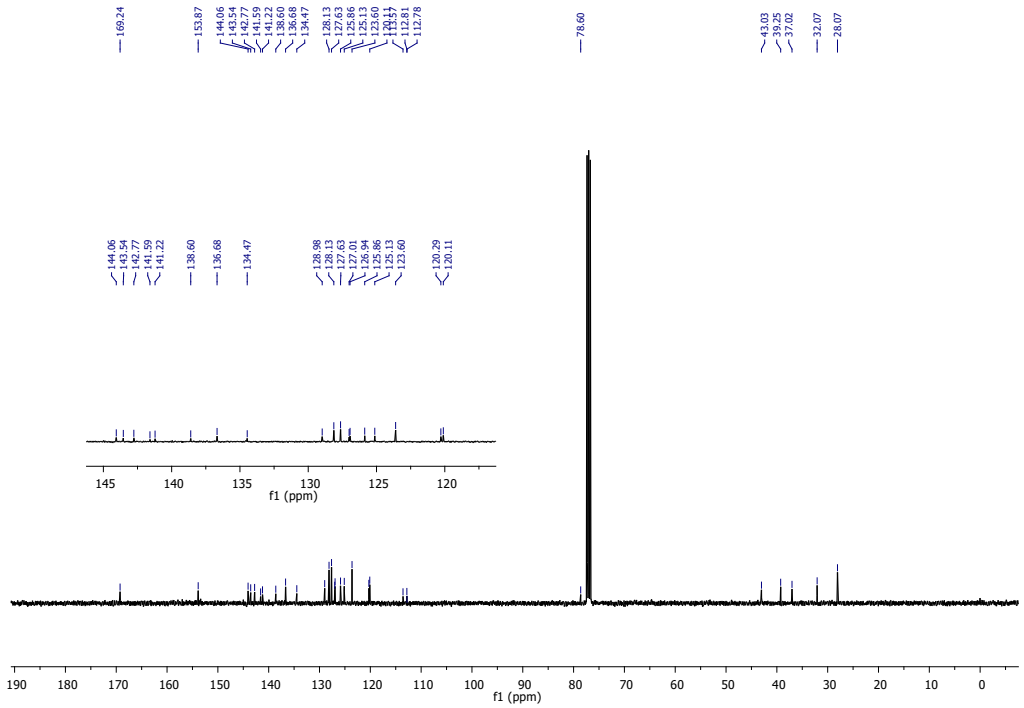

Figure S6. ^{13}C NMR spectrum of K2 (101 MHz, $CDCl_3$).

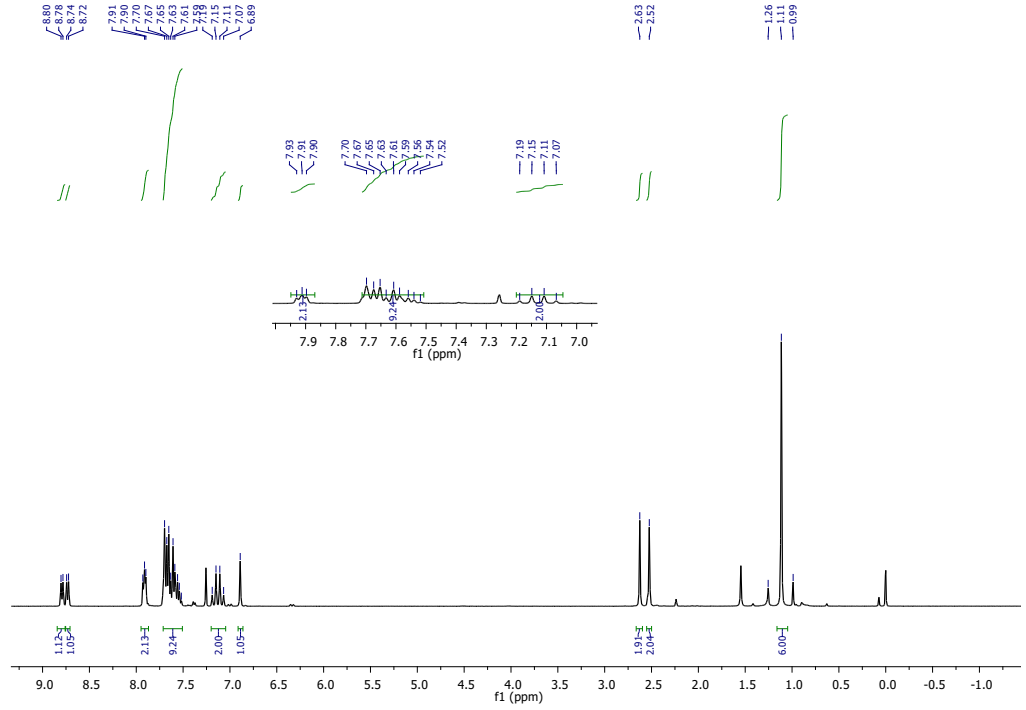

Figure S7. ^{1}H NMR spectrum of K5 (400MHz, $CDCl_3$).

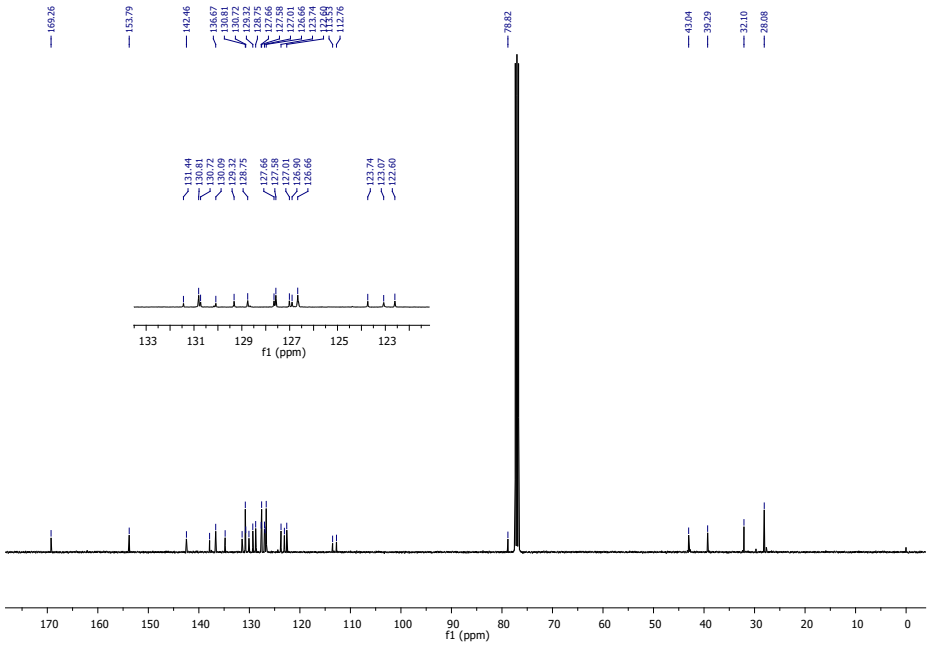

Figure S8. ^{13}C NMR spectrum of K5 (101MHz, $CDCl_3$)

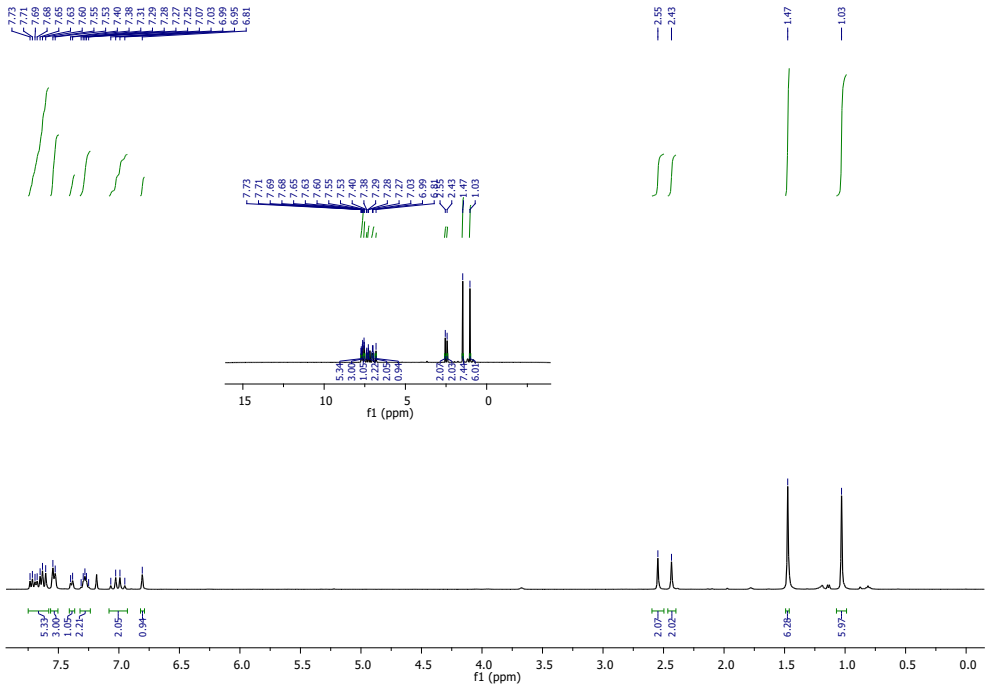

Figure S9. ^{1}H NMR spectrum of K6 (400MHz, $CDCl_3$).

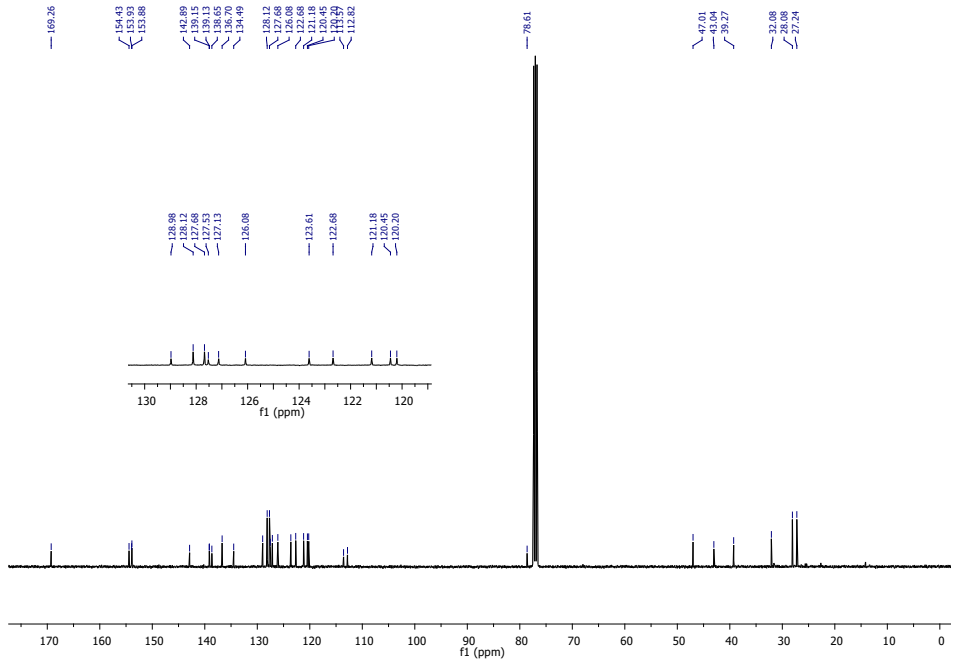

Figure S10. ^{13}C NMR spectrum of K6 (101 MHz, $CDCl_3$).

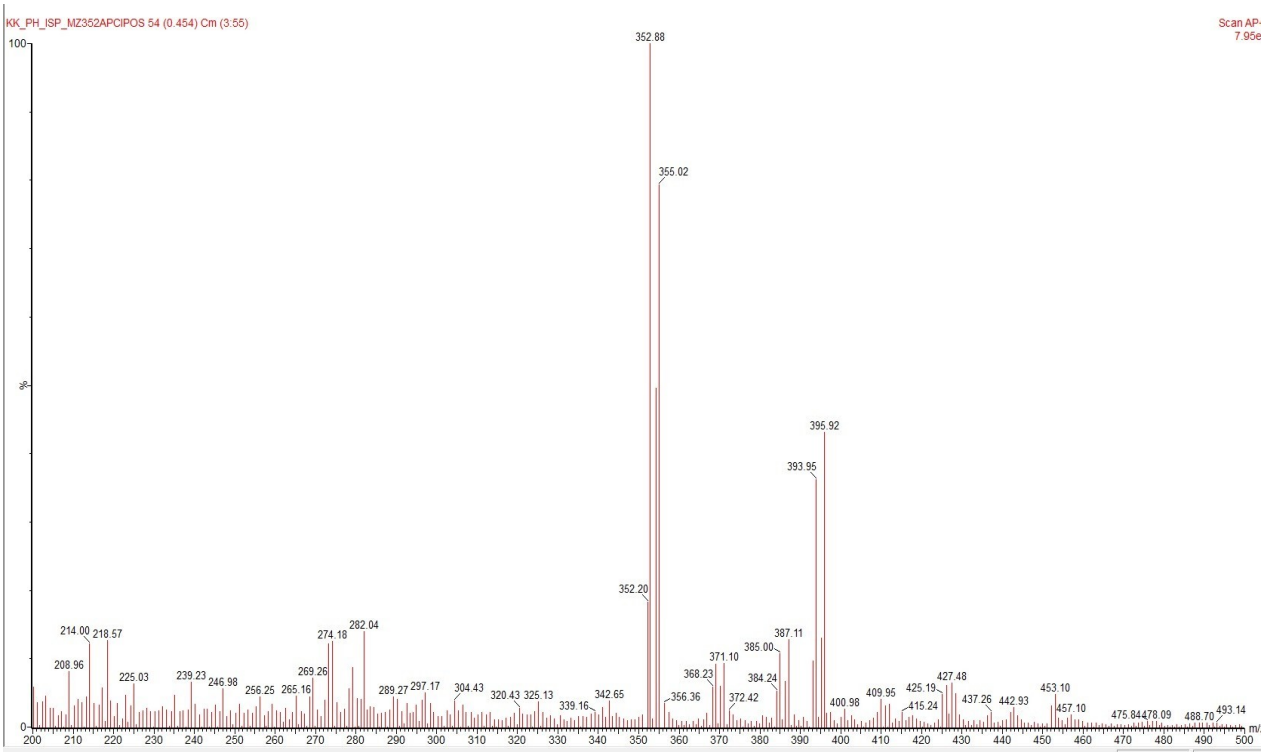

Figure S11. Mass spectrum of Br-Ph-ISP.

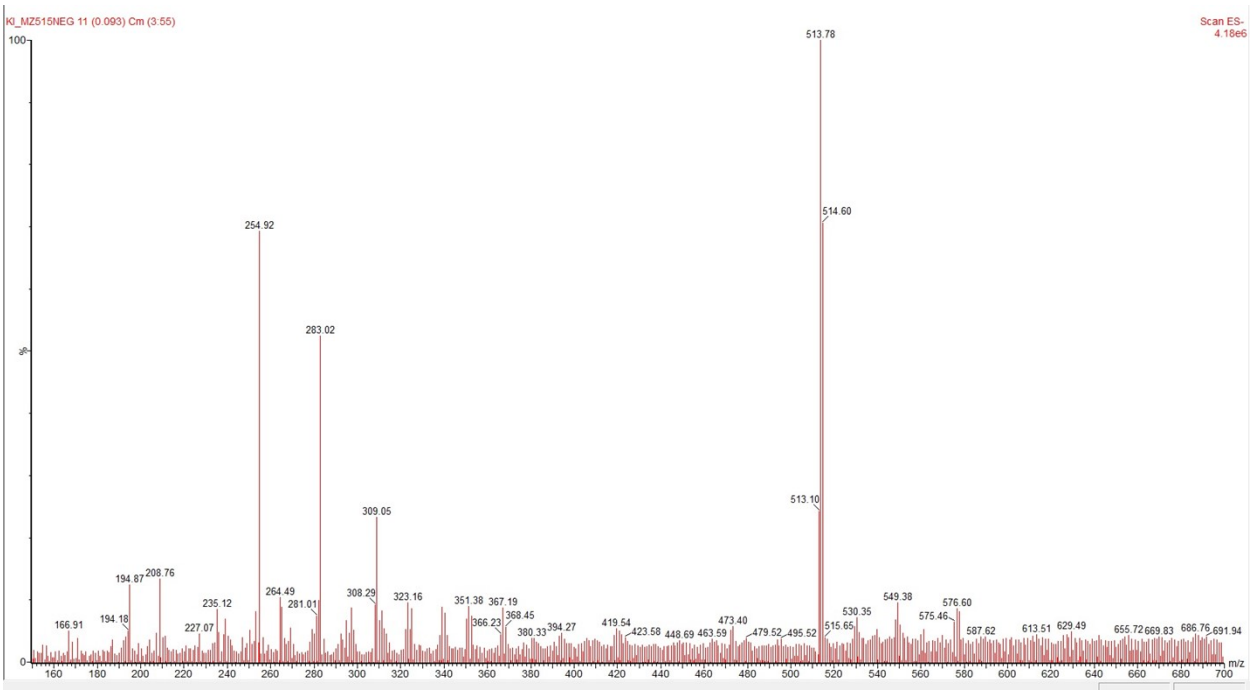

Figure S12. Mass spectrum of K1.

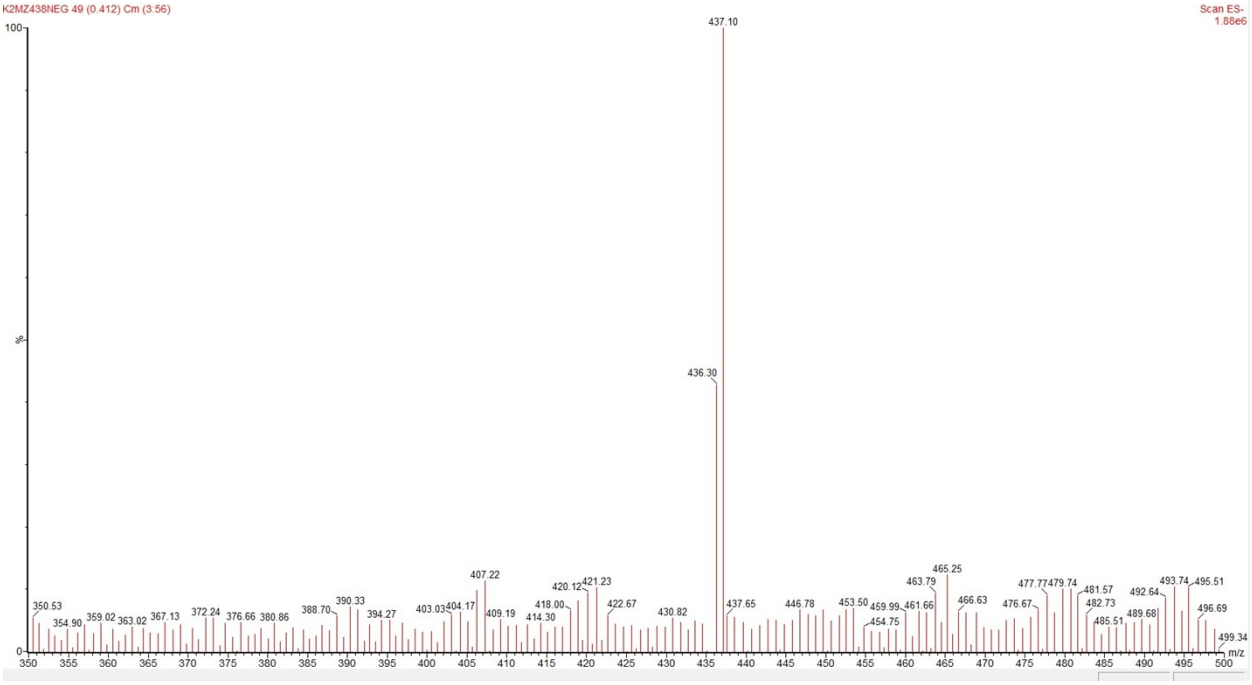

Figure S13. Mass spectrum of K2.

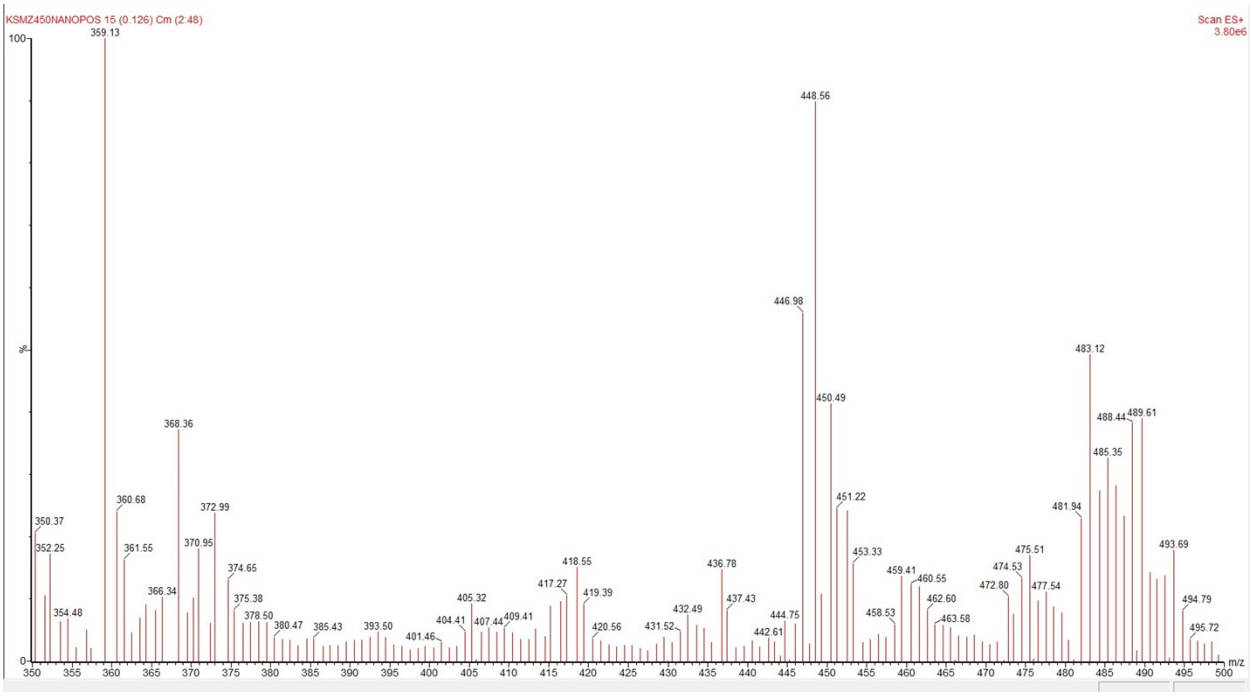

Figure S14. Mass spectrum of K5.

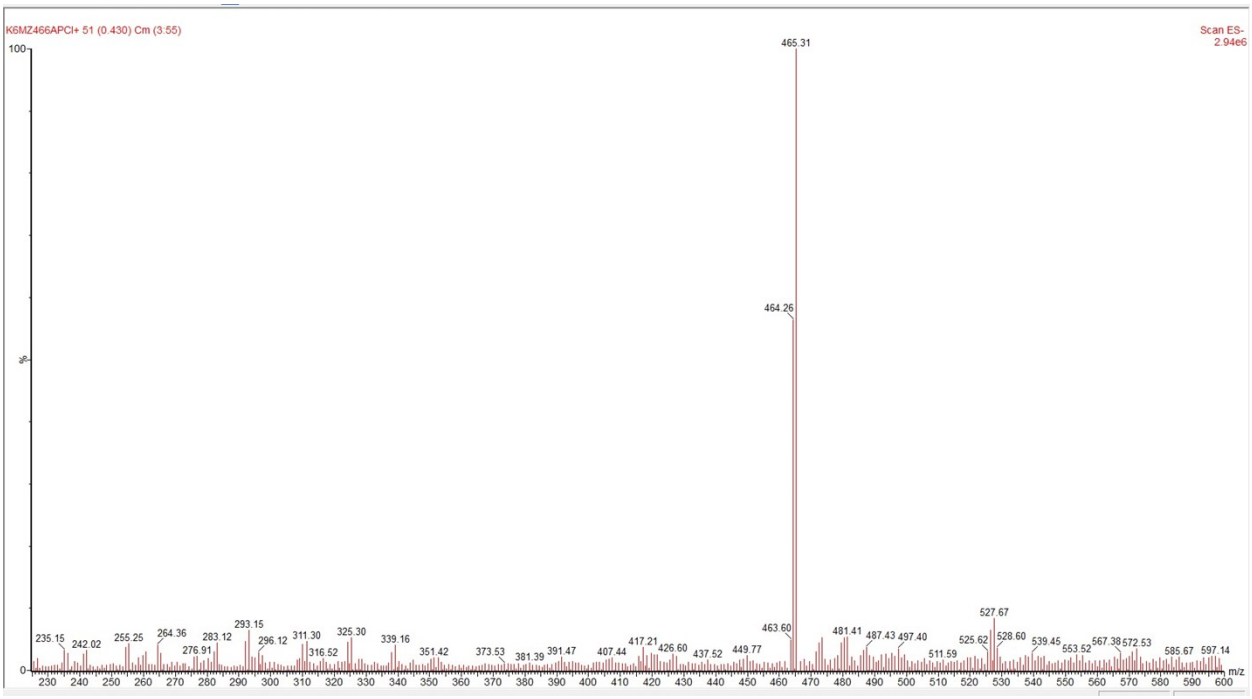

Figure S15. Mass spectrum of K6.

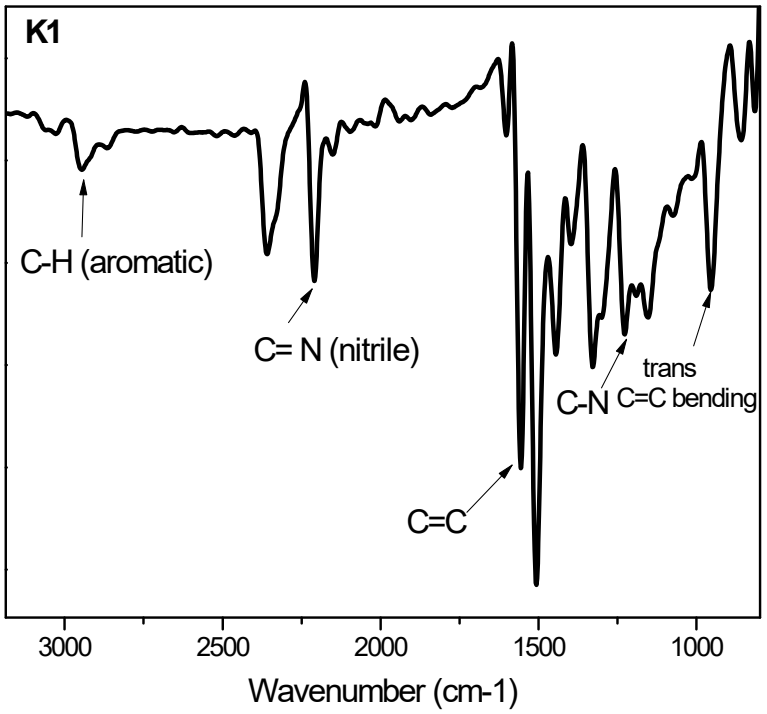

Figure S16. IR spectrum of K1.

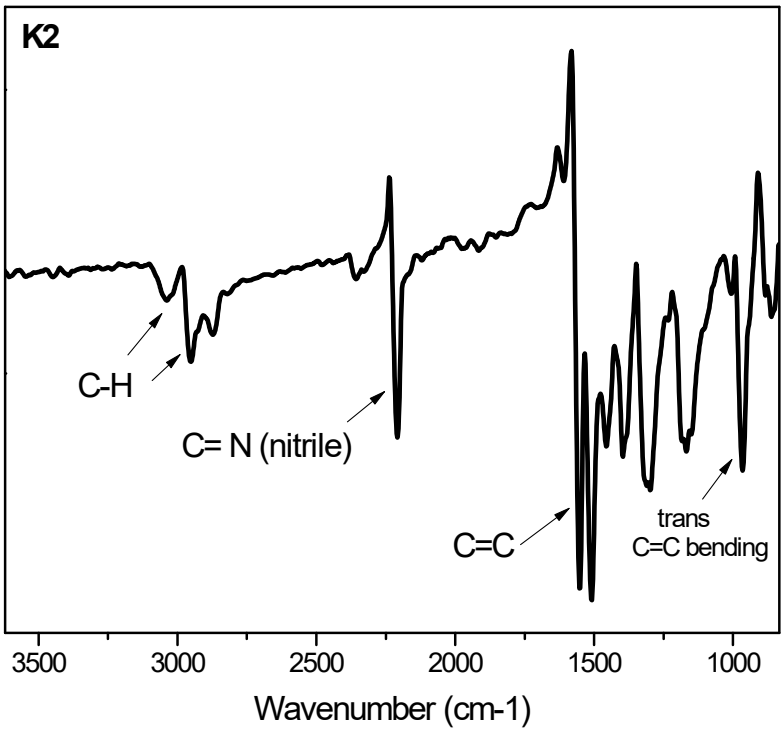

Figure S17. IR spectrum of K2.

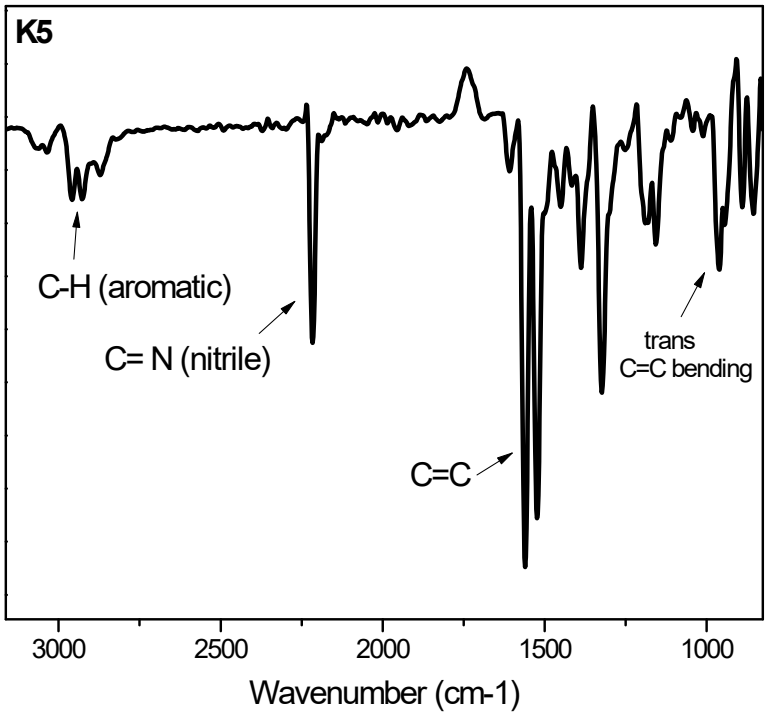

Figure S18. IR spectrum of K5.

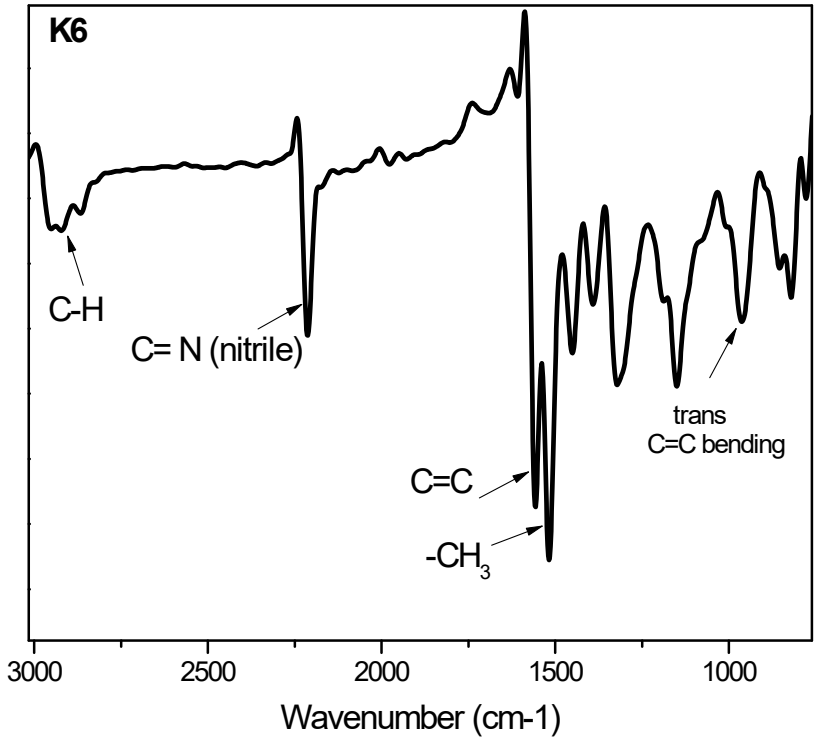

Figure S19. IR spectrum of K6.

S3. Thermal properties.

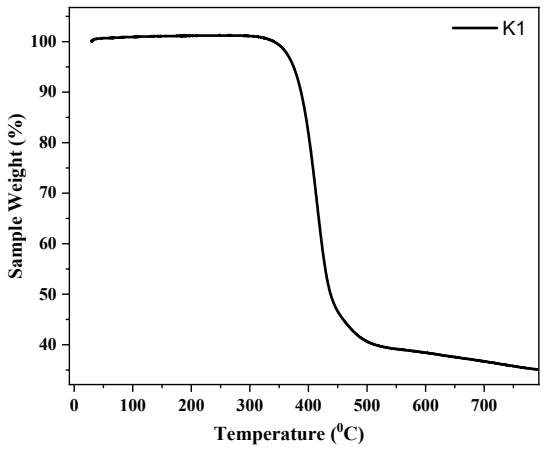

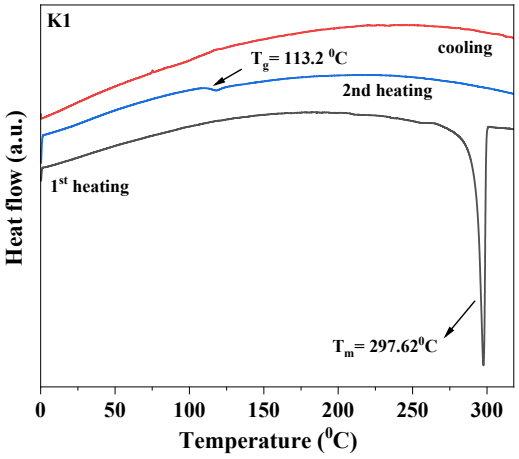

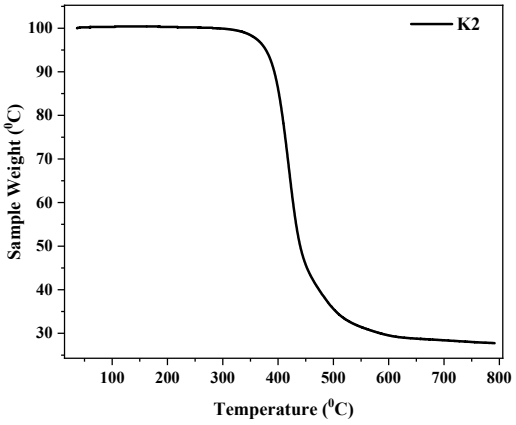

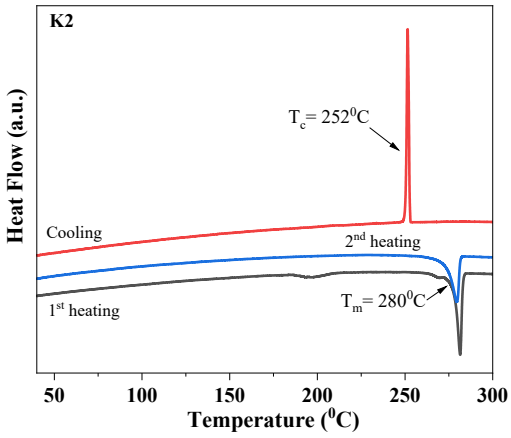

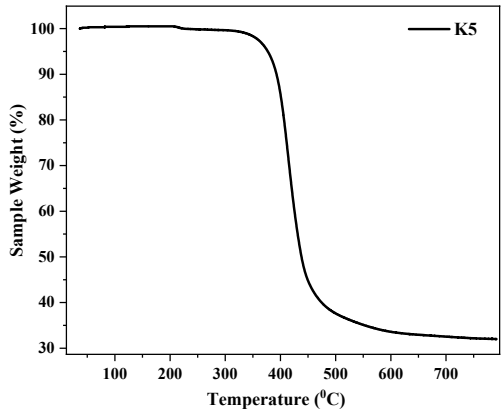

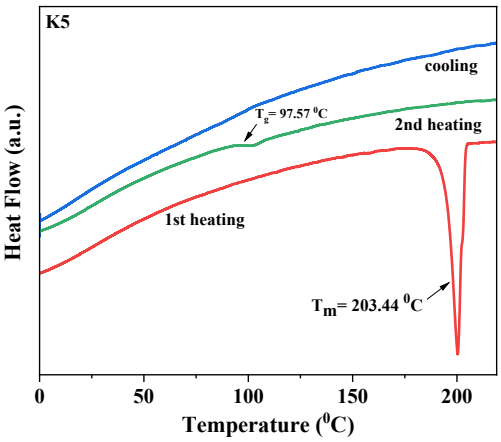

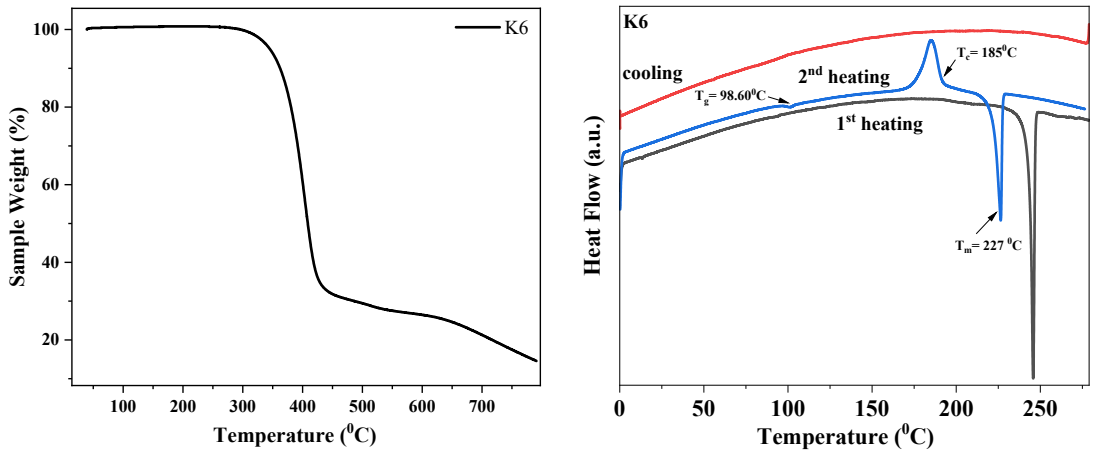

a b

Figure S20. TGA (a) and DSC (b) curves of K1, K2, K5 and K6.

S4. Charge-transporting properties.

As mentioned in the main text, K2 exhibited the highest values of hole and electron mobility based on the TOF and CELIV measurements (Figures S23). TOF current transients indicate very dispersive transport in the case of four compounds, K1, K2, K5 and K6. Because of that, it was not possible to obtain transit times (t_{tr}) for charges in films of compounds K2 and K5 under a wide range of applied positive (for holes) and negative (for electrons) voltages (V) at ITO (Figures S24). The CELIV technique is less sensitive to the dispersity of charge transport than the TOF technique. CELIV current transients showed current maxima at times (t_{max}) (Figures S25). As a result, the t_{tr} and t_{max} values were used to calculate hole and electron mobility values at different electric fields, respectively, using formulas (S1)[2] and (S2)[3].

$$\mu = d^2/Vt_{tr} \quad \text{(S1)}$$

$$\mu = Kd^2/A\ t^2_{max} \quad \text{(S2)}$$

Where d represents the thickness of the vacuum-deposited films. K equals 2/3 or 2, respectively, due to the volume or surface absorption of the laser beam and the subsequent photogeneration of

charges in CELIV samples.[3] *A* represents the parameters of the triangle pulses in the CELIV experiment.

The best experimental mobility values of 3×10^{-5} and 5.3×10^{-5} cm^2/Vs at an electric field of 5.85×10^5 V/cm were obtained for K2, making it the most promising for OLED applications. All compounds generally exhibit low mobility values as electric fields decrease. This observation suggests the selection of appropriate host materials when the compounds are used as OLED emitters.

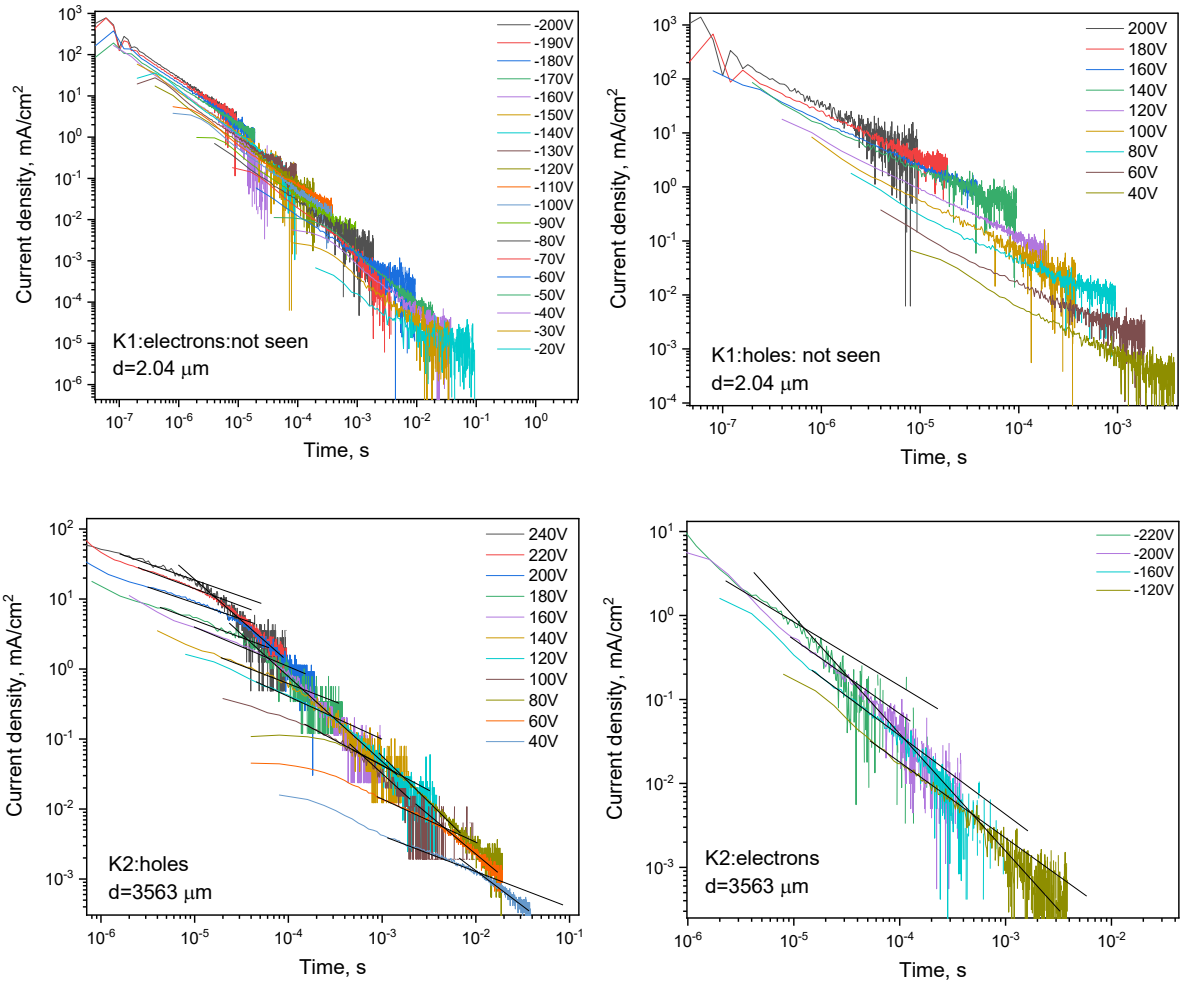

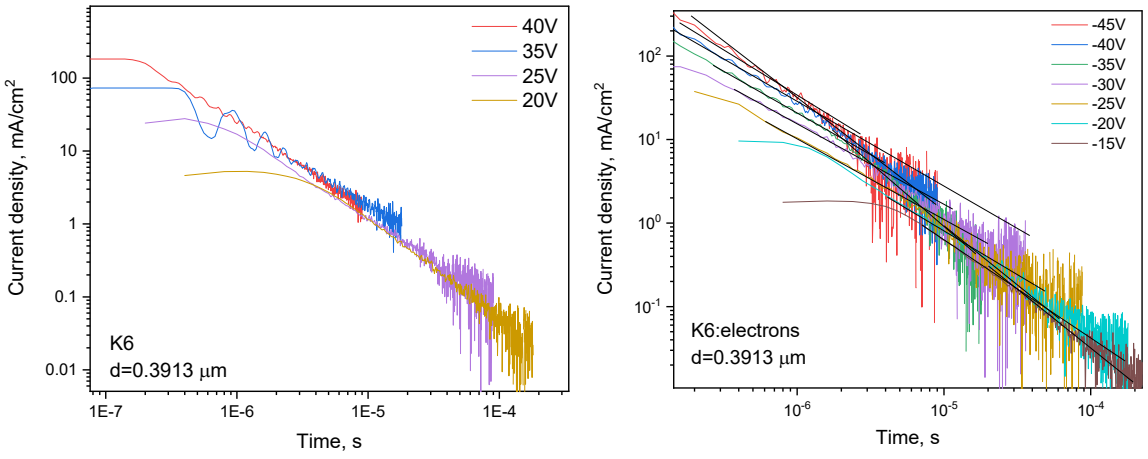

a

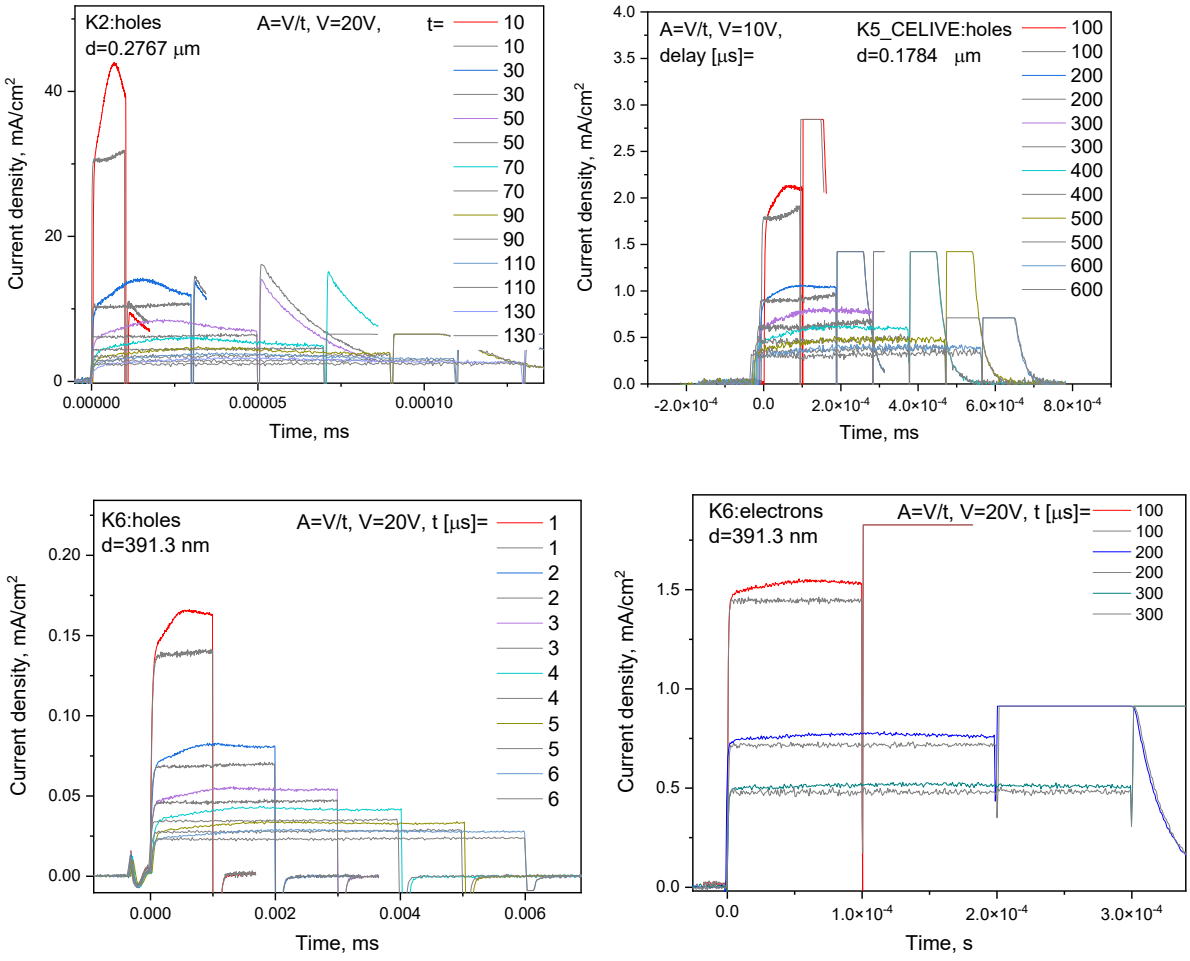

b

Figure S21. TOF (a) and CELIV (b) signals for compounds either K1, K2, K5 or K6.

S5. Photophysical data.

Table S1. Photophysical characteristics derived from neat films of the compounds and the films of the compounds doped in Zeonex (1 wt.%)

Compound	K1	K2	K5	K6
$\lambda_{abs\ film}$, nm	440	423	423	463
$\lambda_{PL\ film}$, nm	595	601	586	576
$\lambda_{PL\ Zeonex}$, nm	548	563	533	530
$\tau_{film\ air}$, ns	1.18	0.67	0.84	1.34
χ^2	1.024	1.011	1.010	1.258
$\tau_{film\ vac}$, ns	1.09	0.59	0.67	1.5
χ^2	1.021	1.060	1.009	1.295
$\tau_{Zeonex\ air}$, ns	1.00	0.89	0.68	0.72
χ^2	1.053	1.046	1.026	1.024
$\tau_{Zeonex\ vac}$, ns	0.98	0.88	0.68	0.74
χ^2	1.021	1.000	1.114	1.173

(a) **(b)**

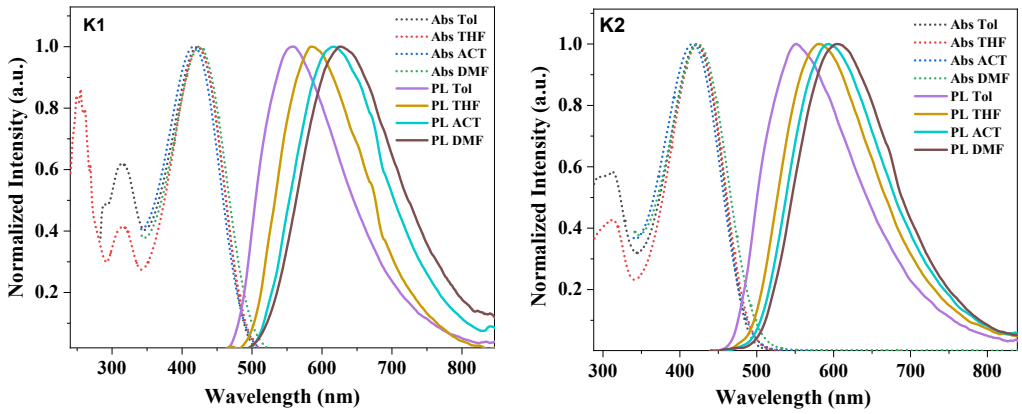

(c) **(d)**

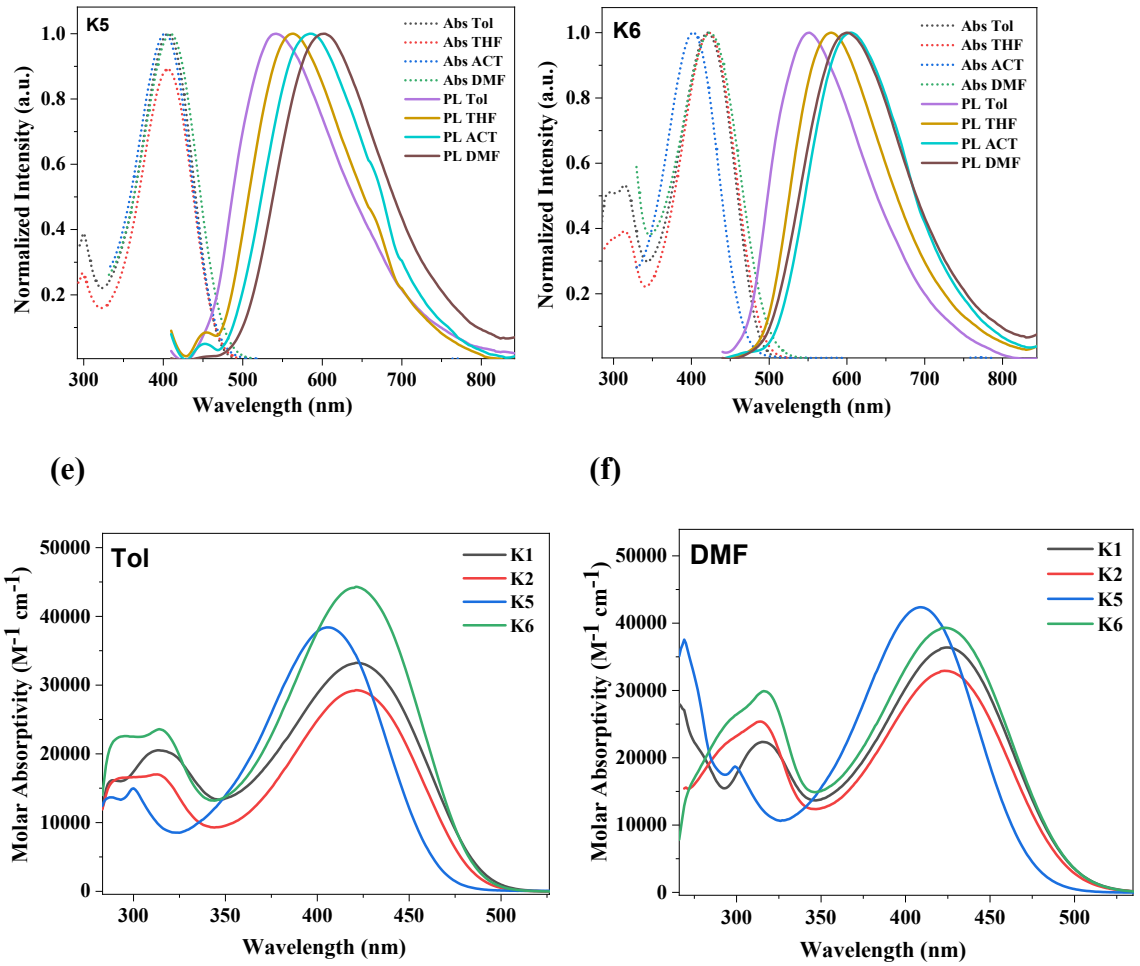

FigureS22. UV-vis and PL spectra (at λ_{exc}= 430 nm, 400 nm respectively) of K1 (a), K2 (b), K5 (c) and K6 (d) for 10^{-5}M solutions of Tol, THF, ACT and DMF, and Molar Absorptivity as a function of absorption wavelength for toluene (e) and DMF (f) solutions K1, K2, K5 and K6 in (1×10^{-5} M) at ambient temperature.

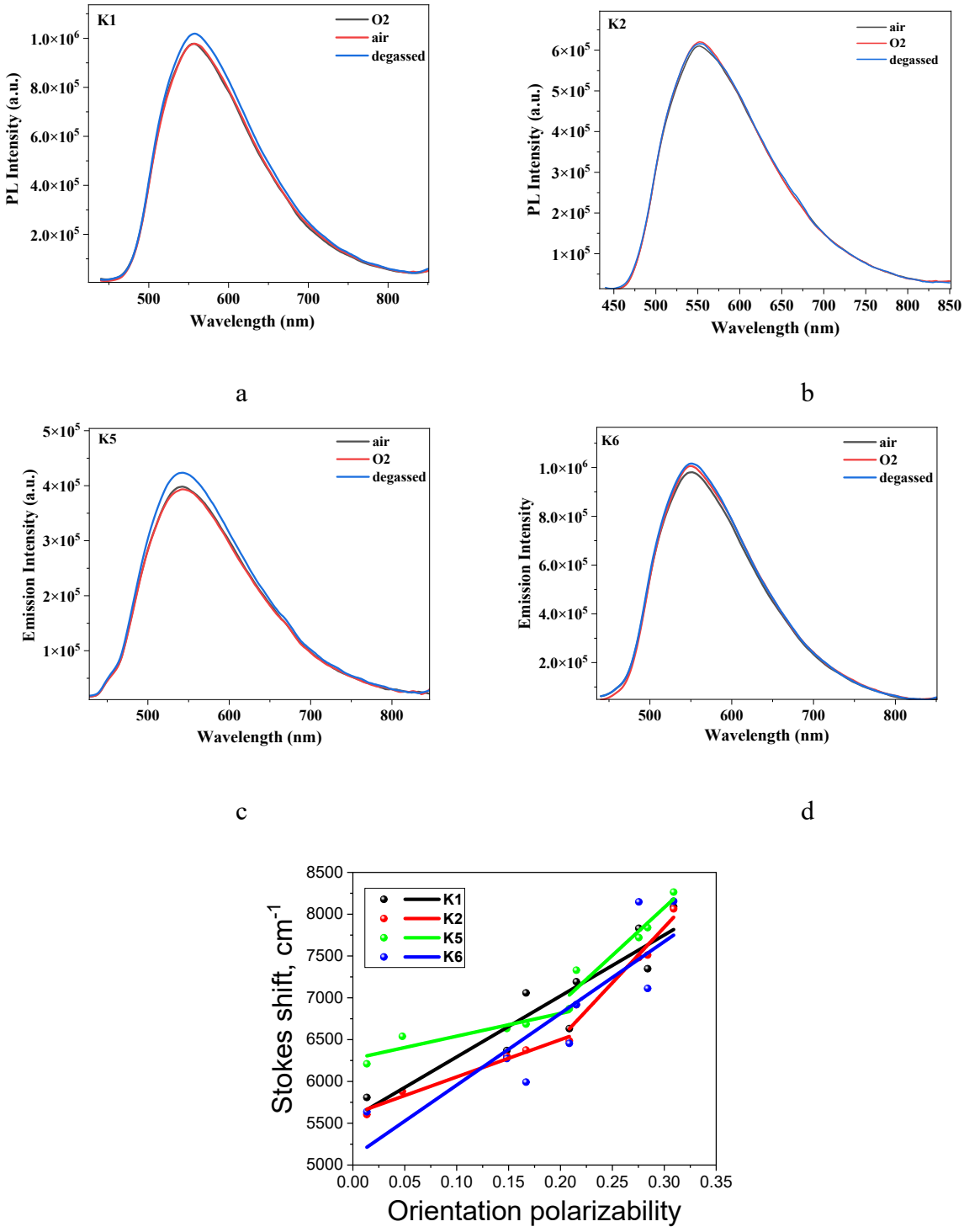

Figure S23. PL spectra of purged with Oxygen, air equilibrated and degassed toluene solutions of K1 (a), K2 (b), K5 (c) and K6 (d). The Lippert-Mataga plot for K1-K6.

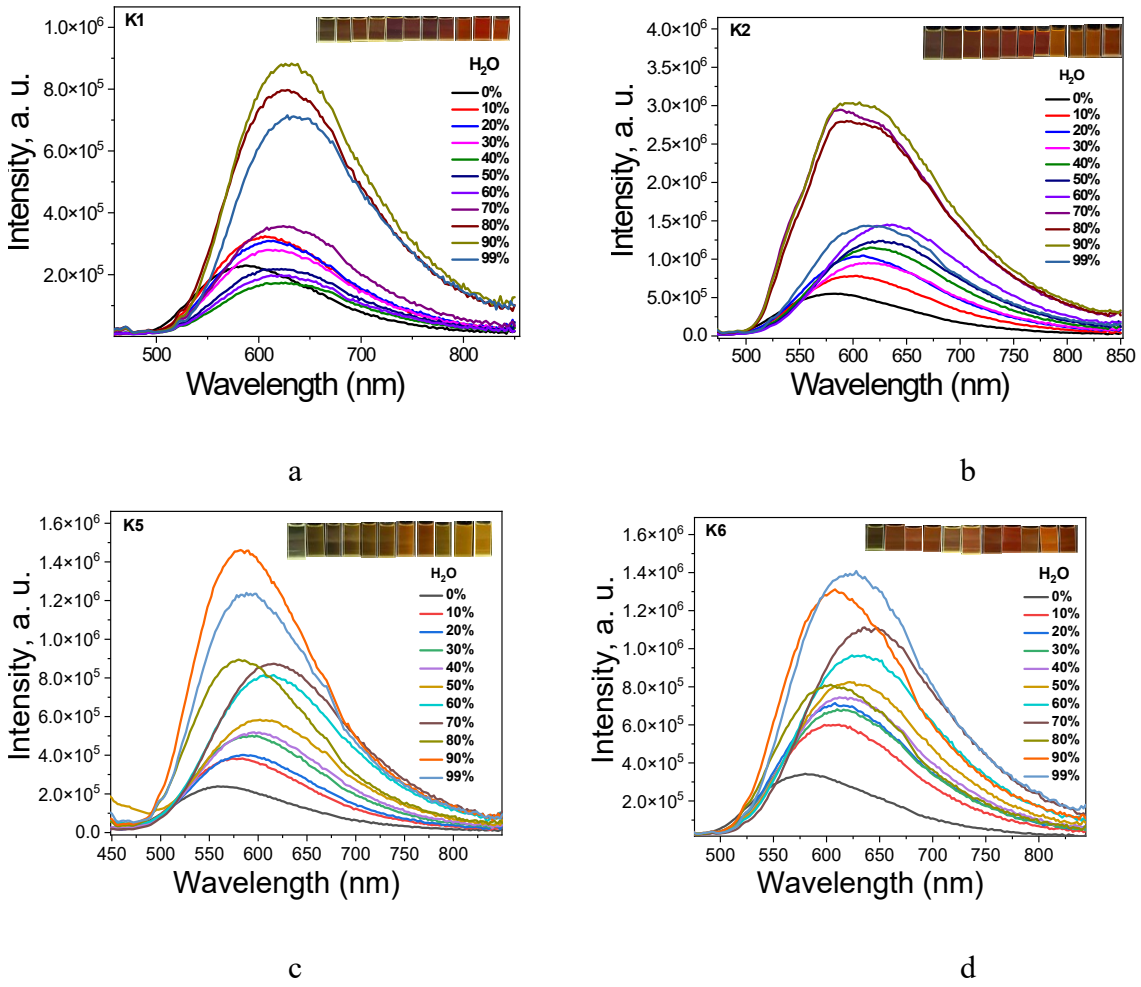

Figure S24. PL spectra of the dispersions of K1 (a), K2 (b), K5 (c) and K6 (d) in the mixtures of THF and water with different water fractions. (Inset: photos of the corresponding cuvettes)

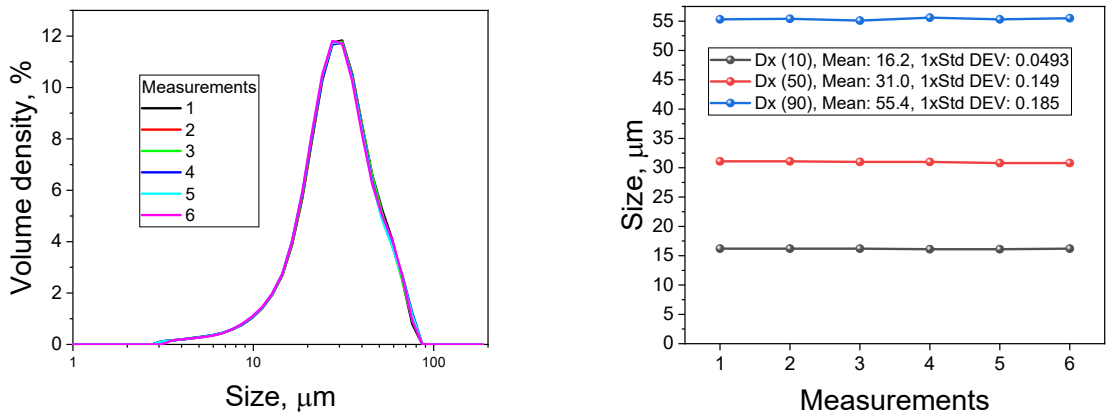

a b

Figure S25. The distribution of the size of the aggregates of K2 in the mixture of water (volume fraction of 99%) and THF (volume fraction of 1%) (a) and the corresponding data of the mean values and errors (b).

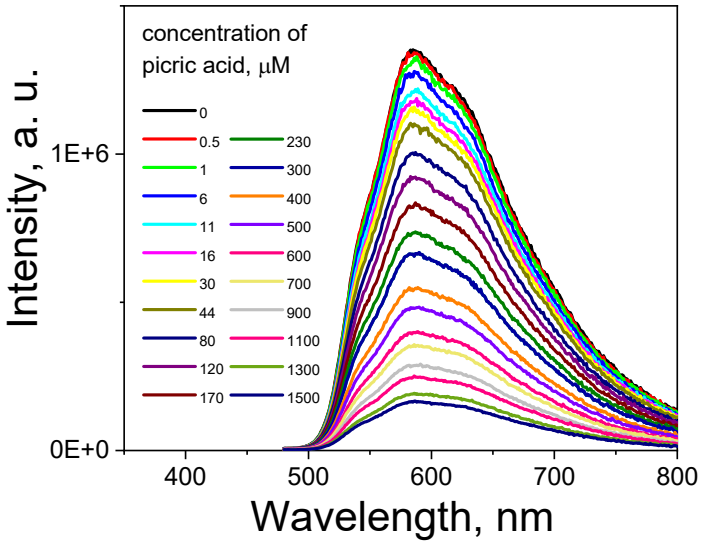

Figure S26. PL spectra of the dispersions of K2 (10^{-4} M) and picric acid in the mixtures of THF and water with the volume fraction of water of 95%

S6. Theoretical data

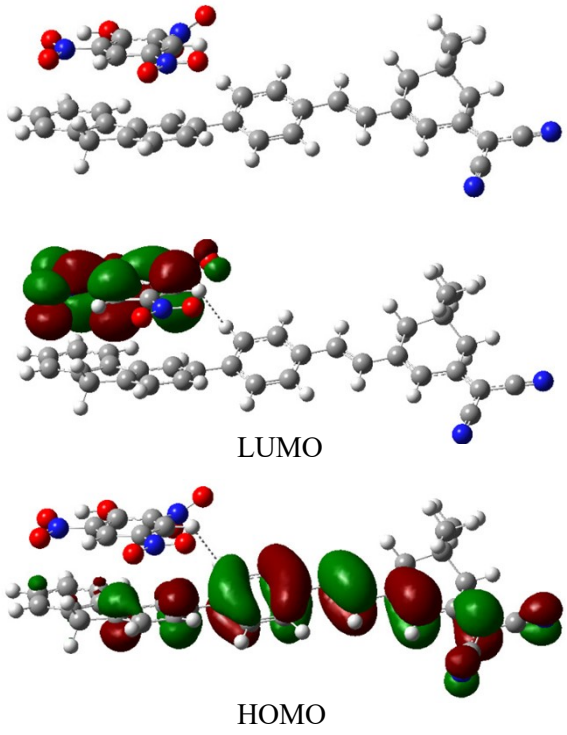

Figure S27. Interaction of K2 with picric acid and their molecular orbitals.

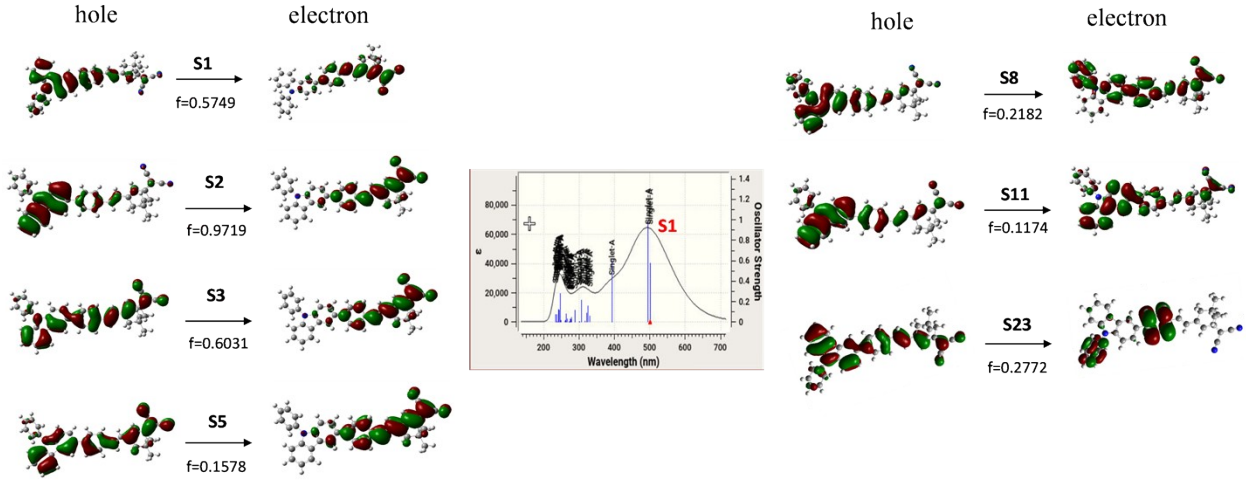

Figure S28**.** Natural transition orbitals for main transition configuration of compound K1 and theoretical UV spectra depicting main transitions (in middle) obtained from TD-DFT (for toluene) (B3LYP, 6-31G(d,p))**.**

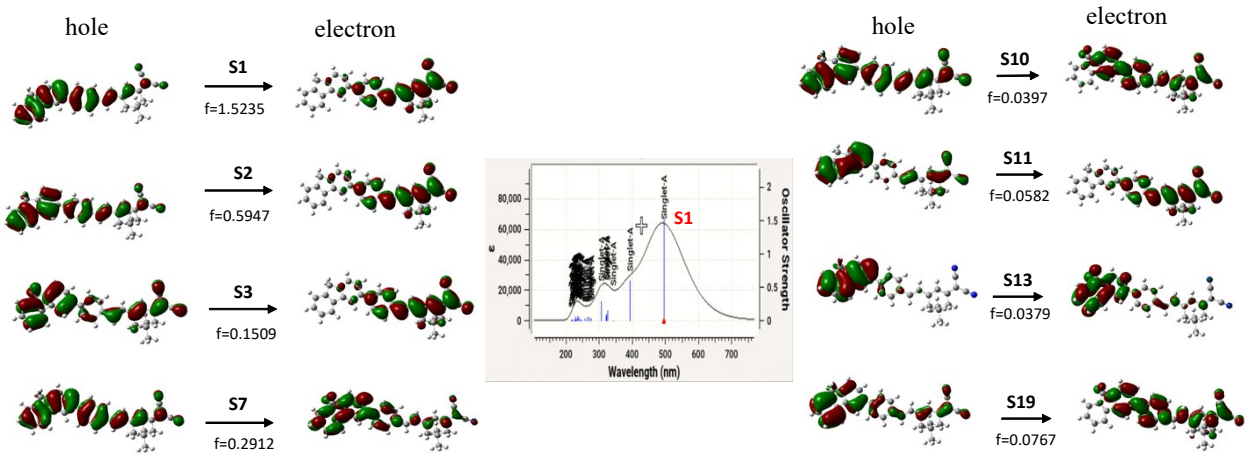

Figure S29. Natural transition orbitals for main transition configuration of compound K2 and theoretical UV spectra depicting main transitions (in middle) obtained from TD-DFT (for toluene) (B3LYP, 6-31G(d,p)).

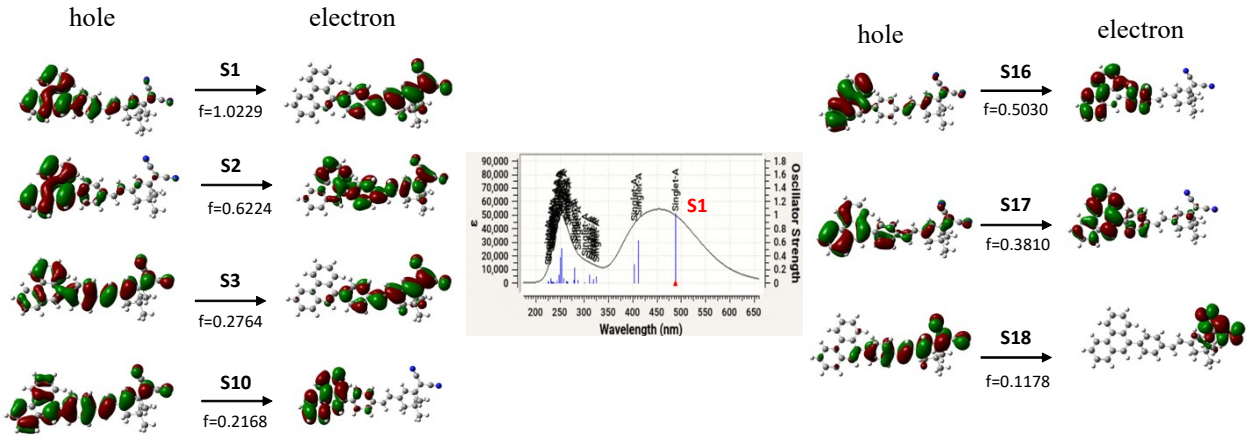

Figure S30. Natural transition orbitals for main transition configuration of compound K5 and theoretical UV spectra depicting main transitions (in middle) obtained from TD-DFT (for toluene) (B3LYP, 6-31G(d,p)).

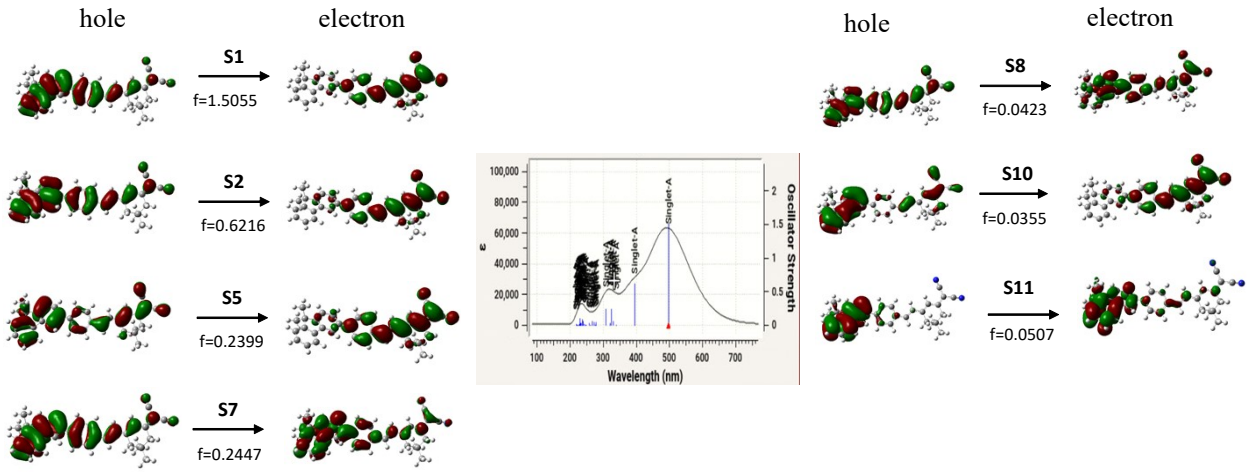

Figure S31. Natural transition orbitals for main transition configuration of compound K6 and theoretical UV spectra depicting main transitions (in middle) obtained from TD-DFT (for toluene) (B3LYP, 6-31G(d,p))**.**

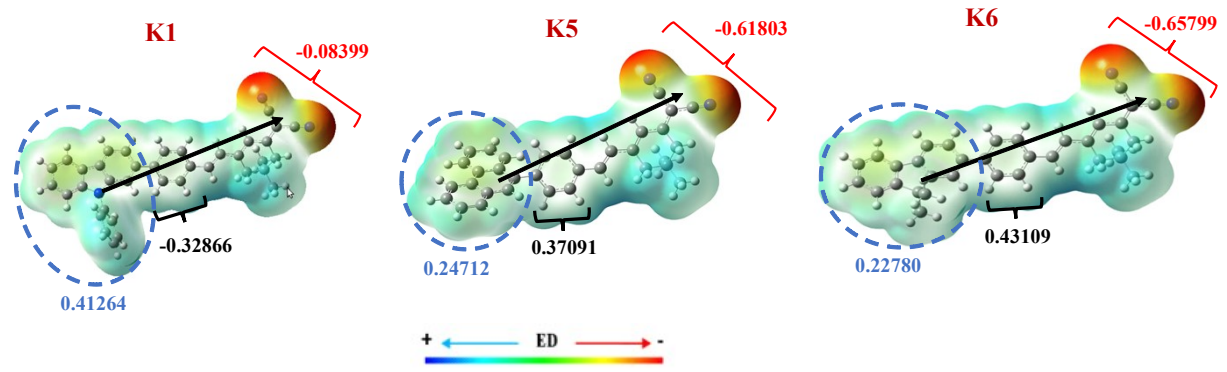

Figure S32. Electrostatic potential maps (B3LYP, 6-31G(d,p) (isosurface value 0.002) of the ES of molecules K1, K5 and K6. Atom color codes: C =gray; H =white; N =blue and O =red, S =yellow (ED: electron density), the direction of dipoles is also presented.

S7. Electroluminescence and comparison with other compounds.

Table S2a. EL data of the WOLED.

Voltage, V	1931 $CIE_{x,y}$	1960 $CIE_{u,v}$	1976 $CIE_{u',v'}$	CCT, K	CRI
8	(0.35, 0.38)	(0.20, 0.33)	(0.20, 0.50)	4910	82
10	(0.36, 0.40)	(0.20, 0.34)	(0.20, 0.51)	4770	78
12	(0.36, 0.40)	(0.20, 0.34)	(0.20, 0.51)	4720	77
14	(0.36, 0.41)	(0.20, 0.34)	(0.20, 0.51)	4640	78

CCT - correlated color temperature; CRI - color rendering index

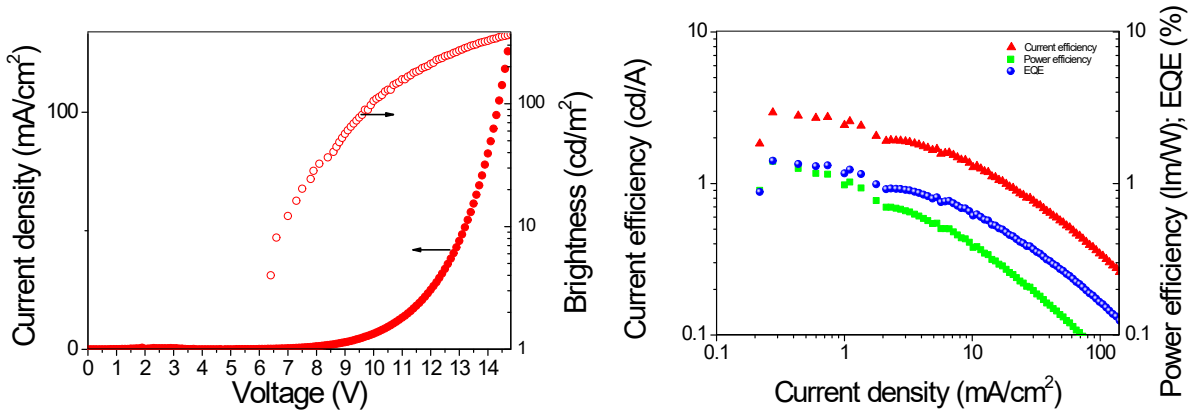

Figure S33. Current density/brightness – voltage plot (a); Current efficiency / power efficiency / EQE – current density plot (b).

Table S2b. Comparison of the characteristics of K2 with other compounds

Compound	λ, nm	$K_{SV\ picric\ acid\ sensor}$, M^{-1}	$PLQY_{sol}$, %	$PLQY_{film}$, %	EQE_{WOLED}, %	1931 $CIE_{x,y\ WOLED}$
K2	601	16.2×10^4, 2.7×10^3	ca. 0	7	1.4	(0.35, 0.38)
1c [4]	588	5.94×10^4	-	-	-	-
R1 [5]	496	4.37×10^4	-	-	-	-
3c [6]	500	4.31×10^{-4}	-	-	-	-
mmCTPI [7]	493	-	1	24	2.3	(0.21, 0.34)
TCz-F [7]	490	-	1	18	1.1	(0.19, 0.32)
S-BN-tCz [7]	488	-	67	48	0.7	(0.32, 0.45)
R-BN-tCz [7]	488	-	-	-	1.6	(0.31, 0.45)
2 [8]	476		1	28	0.5	(0.23, 0.31)
P7 [9]	550	-	-	-	14.1	(0.31, 0.42)

S8. Quadratic hyperpolarizability.

$$\beta \propto \Delta\mu_{ge}\, r_{ge}^2 / (E_{ge})^2 \quad \text{…….. (1)}$$

where β =first hyperpolarizability, $\Delta\mu_{ge}$ =difference in the ground and excited state dipole moments, r_{ge} =transition dipole moment, a measure of oscillator strength (f) or molar extinction coefficient (ε) and E_{ge} = excitation energy of the ICT band.

$$\beta_o = \beta\left[1 - \left(\frac{\lambda_{max}}{\lambda_{ex}}\right)^2\right]\left[1 - \left(\frac{\lambda_{max}}{\frac{\lambda_{ex}}{2}}\right)^2\right] \quad \text{.....(2)}$$

$$\beta_{zzz} = \frac{\beta_{\mathrm{HRS}}}{\sqrt{\frac{6}{35}}} \quad \text{... ... (3)}$$

$$\rho\left(\frac{<\beta_{ZZZ}^2>}{<\beta_{XZZ}^2>}\right)(\mathrm{Rp})^{-1} \text{.....(4)}$$

TableS3. The estimated Natural Bond Orbital (NBO) charge distribution over donor (D), acceptor (A) and π-linker units and calculated dipole moments of **K1-K6** in ground (GS) and excited (ES) states.

	NBO Charges[a]				**Dipole moments (D)**[b]		
	D	**π**	**A**	**Δq_D**	**μ_g**	**μ_e**	**$\Delta\mu$**
K1	0.01858	-0.30942	-0.13229	0.39406	13.13	43.56	30.43
	(0.41264)	(-0.32866)	(-0.08399)				
K2	0.06130	0.13439	-0.19569	0.16602	11.94	29.81	17.87
	(0.22732)	(0.27896)	(-0.50627)				
K5	0.08961	0.23616	-0.32577	0.15751	11.32	35.80	24.48
	(0.24712)	(0.37091)	(-0.61803)				
K6	0.13444	0.33259	-0.46732	0.09336	11.96	30.99	19.03
	(0.22780)	(0.43109)	(-0.65799)				

[a]NBO (TD-DFT, B3LYP/6.31G(d,p) level) in the ground and excited states (in parentheses) Δq_D is difference between electronic charges of donor in GS and ES; [b]μ_g and μ_e are calculated ground and excited state dipole moments (TD-DFT, B3LYP/6.31G (d,p) level in toluene, respectively. $\Delta\mu$ is the difference in ground and excited state dipole moments.

Table S4. Experimental and theoretical UV-visible absorption data of **K1-K6**.

	Experimental data	**TD-DFT calculated**[c,d]

	$\lambda^{max}/\varepsilon_{max}$[a,b]	λ^{max}_{theo}	CI[e], Contribution	*f*, ΔE
K1	425/32984 (2.50, D→A)	495	0.70374, H-1→L, 99%	0.9719, 2.65
K2	424/29166 (2.54, D→A)	393	0.69909, H-1→L, 98%	0.5947, 2.92
K5	408/38511 (2.65, D→A)	412	0.65551, H-1→L, 86%	0.6224, 2.87
		403	0.66090, H-2→L, 87%	0.2764
K6	424/44054 (2.55, D→A)	395	0.69907, H-1→L, 98%	0.6216, 2.91

[a]Recorded in Toluene (1×10^{-5} M), ε_{max} in $M^{-1}cm^{-1}$; [b]In parenthesis: optical band gap in eV (E_g^{opt} = 1239.84187/λ_{edge}) and assignment; [c]calculated using TD-DFT (Gaussian 16) calculations performed at B3LYP/6-31G(d,p)/CPCM model in toluene and only CT band is shown; [d]calculated for the lowest 30 excited states and only energies above 300 nm with *f* greater than 0.1 are shown, *f* = oscillator strength, CI = configurational interaction, ΔE = Energy difference between HOMO (H) and LUMO (L) in eV (refer to table 2); [e]main contribution and assignment.

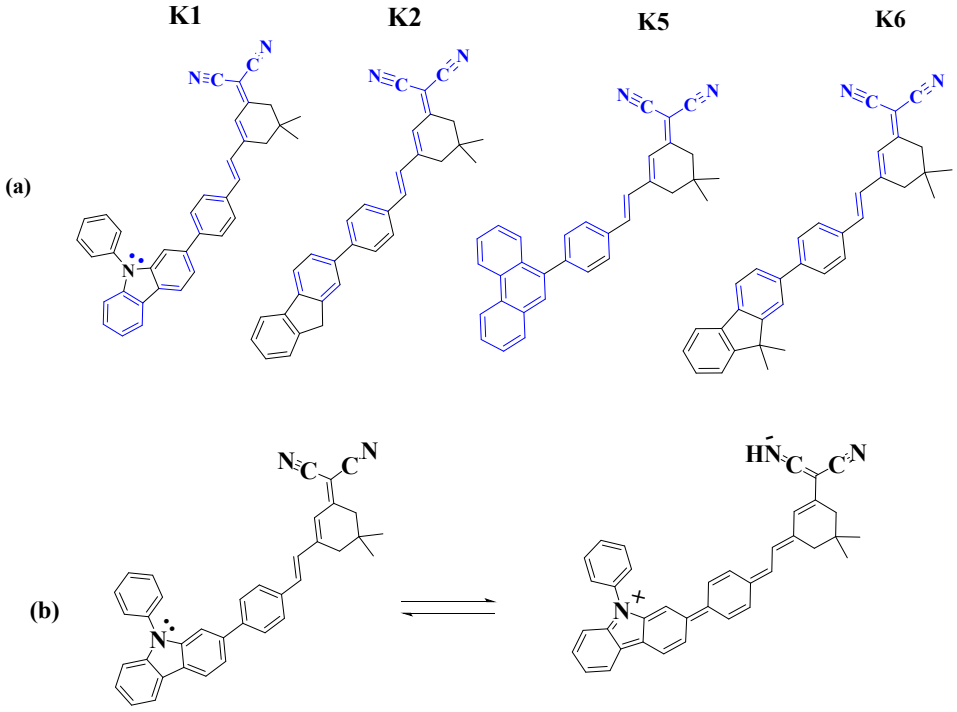

Figure S34. Illustration of the polarizable electrons involved in ICT within the D-A motifs **(a)**, possible aromatic and quinoid like structures of K1 **(b)**

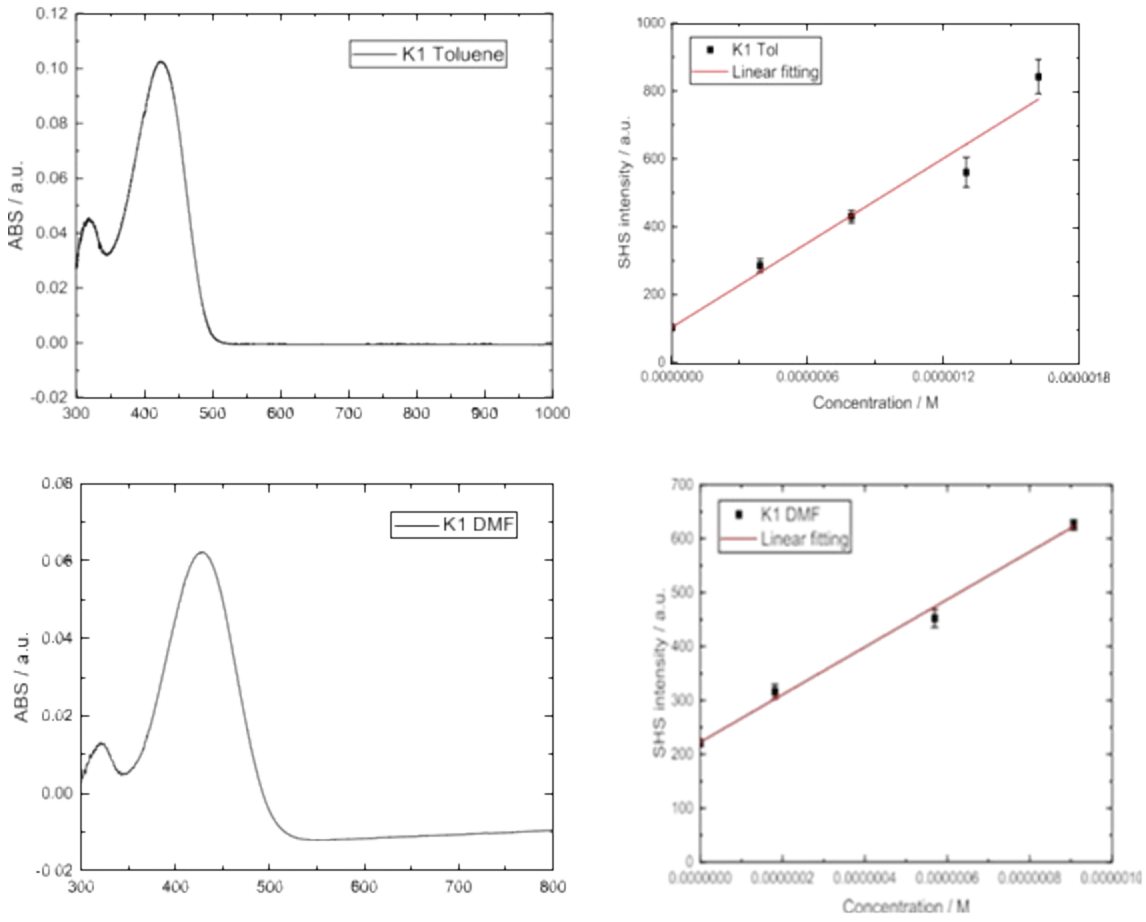

Figure S35. Absorption profiles and concentration dependence (with concentration of series: C0: 0μM (pure solvent) C1: 0.970μM C2: 1.94μM C3: 2.91μM C5: 4.85μM) of first hyperpolarizability of **K1** in toluene and DMF.

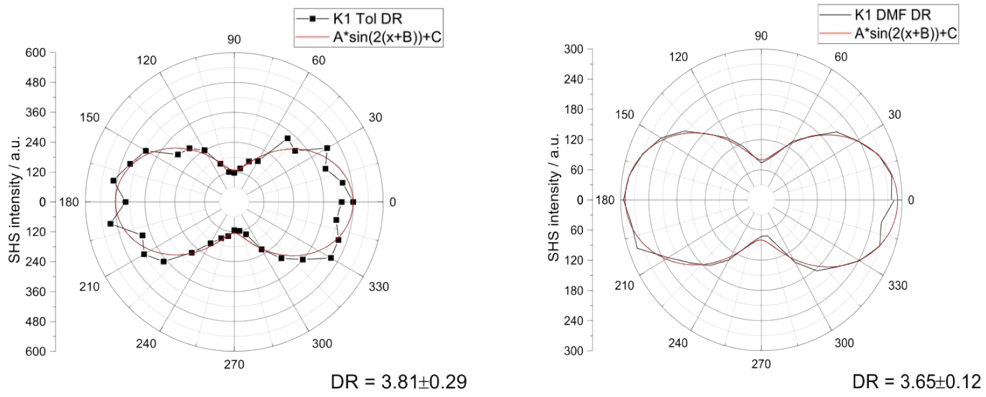

Figure S36. Depolarization ratios of **K1** in toluene and DMF at intensity 1240mW and integration time 2s (K1) 5s (Tol), 3s (K1) 5s (DMF).

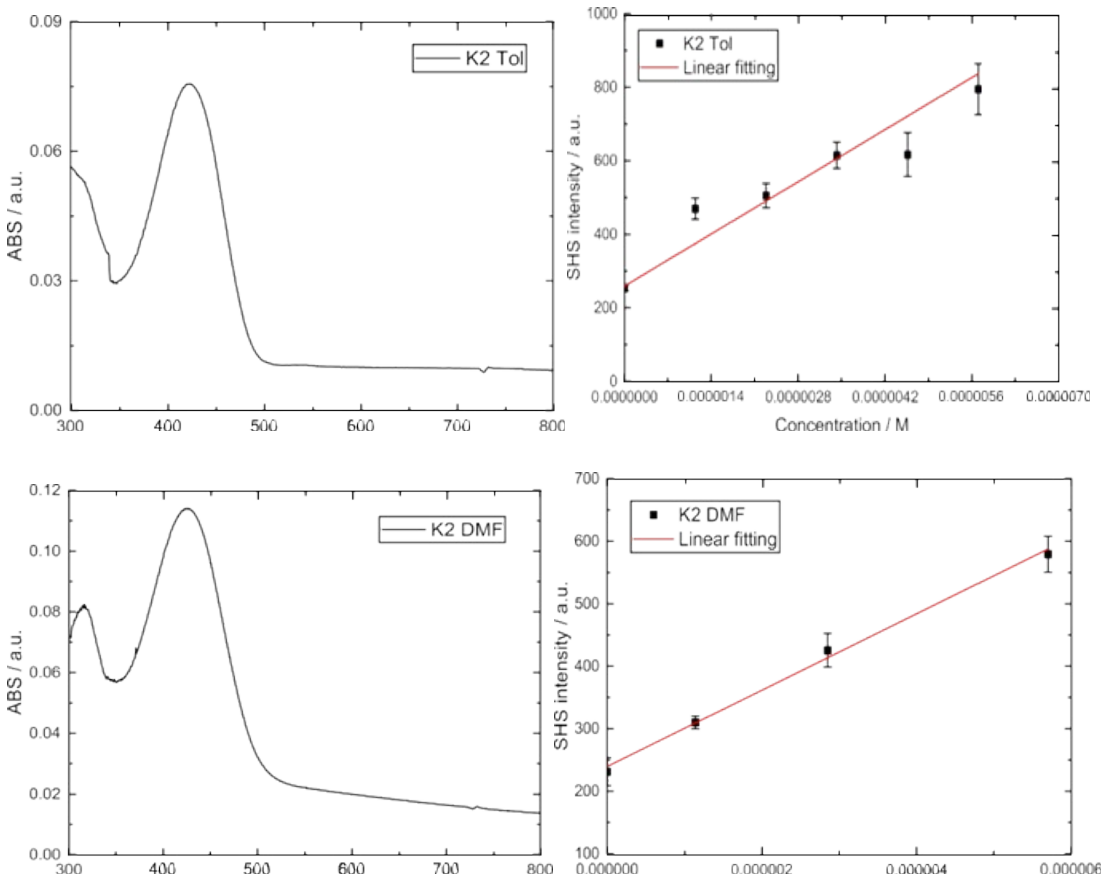

Figure S37. Absorption profiles and concentration dependence (with concentration of series: **C0:** 0 μM (pure solvent) **C1:** 1.14 μM **C2:** 2.28 μM **C3:** 3.42 μM **C4:** 4.56μM **C5:** 5.70 μM) of first hyperpolarizability of **K2** in toluene and DMF.

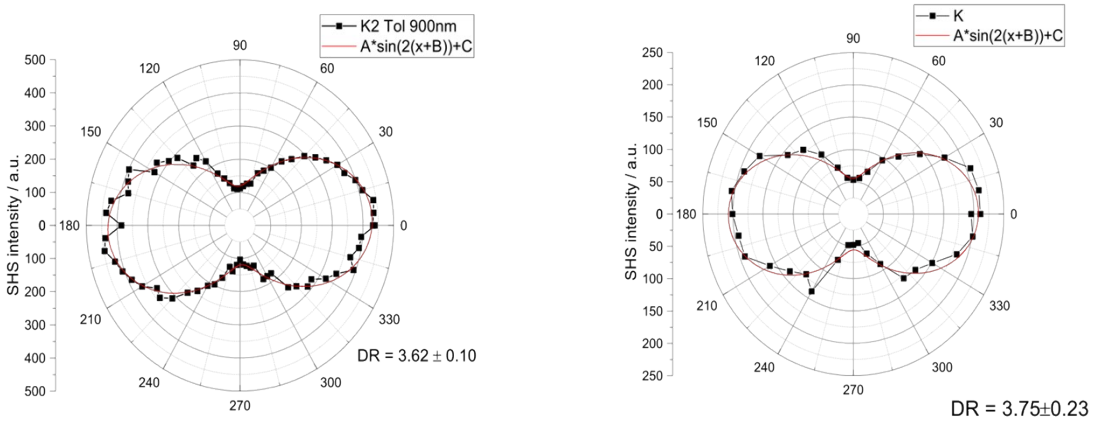

Figure S38. Depolarization ratios of **K2** in toluene and DMF at intensity 1540mW and integration time 5s (Tol), 3s (K2) 5s (DMF).

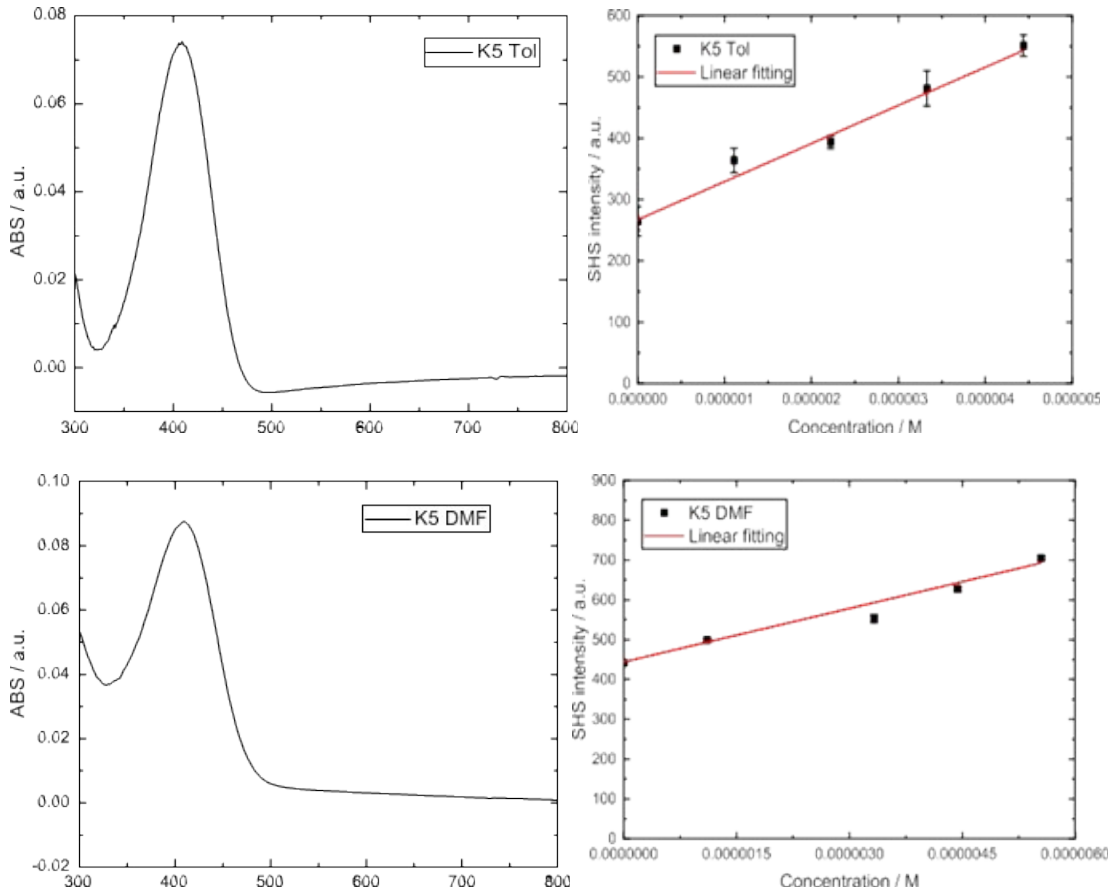

Figure S39. Absorption profiles and concentration dependence (with concentration of series C0: 0 μM (pure Toluene) **C1:** 1.11μM **C2:** 2.22 μM **C3:** 3.33 μM **C4:** 4.44 μM)of first hyperpolarizability of **K5** in toluene and DMF.

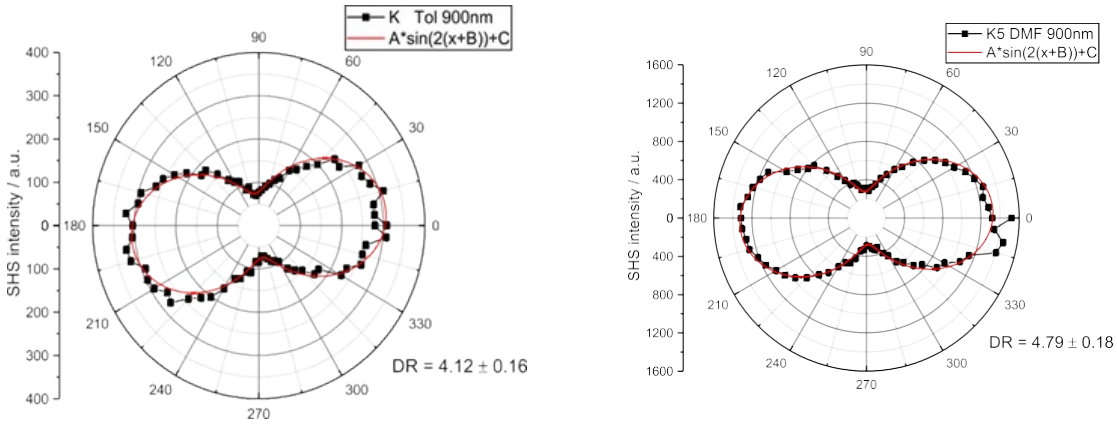

Figure S40. Depolarization ratios of **K5** in toluene and DMF at intensity 1540mW and integration time 5s (Tol), 5s (DMF).

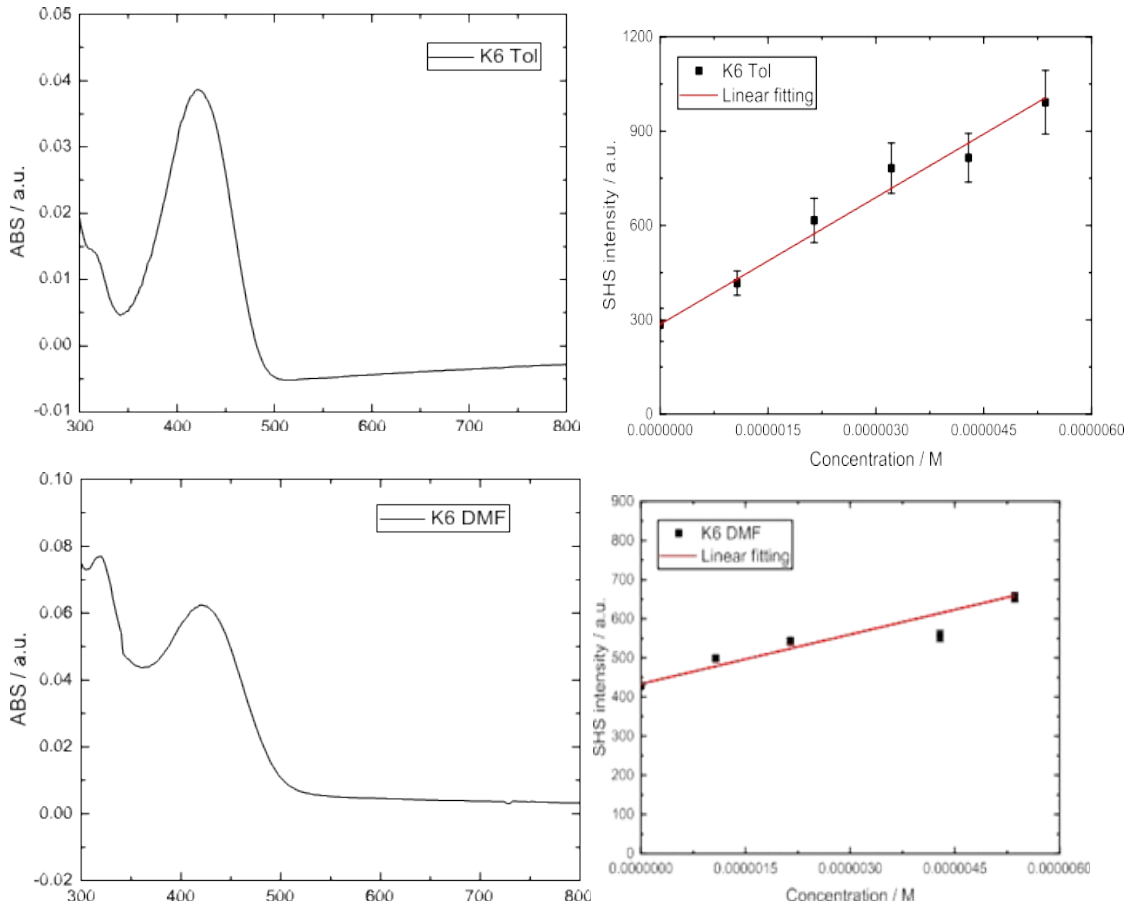

Figure S41. Absorption profiles and concentration dependence (with concentration of series C0: 0 μM (pure Toluene) **C1:** 1.07μM **C2:** 2.14 μM **C3:** 3.21 μM **C4:** 4.29 μM **C5:** 5.36 μM of first hyperpolarizability of **K6** in toluene and DMF.

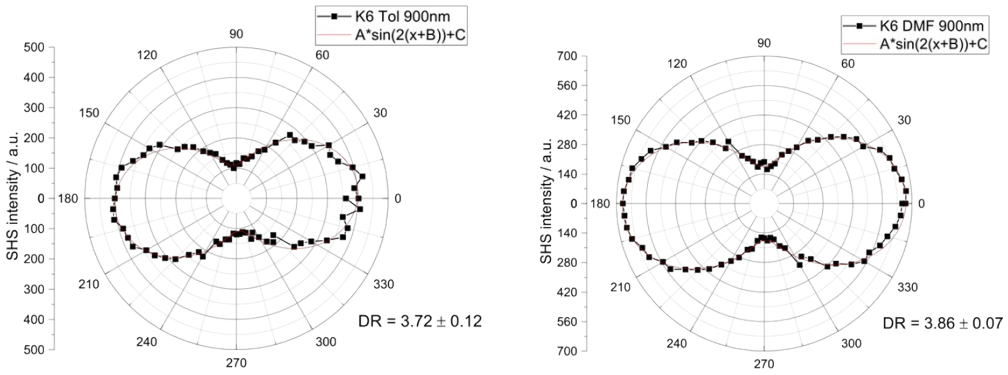

Figure S42. Depolarization ratios of **K6** in toluene and DMF at intensity 1540mW and integration time 5s (Tol), 35s (DMF).

S9. References

1 M. J. Frisch, G. W. Trucks, H. B. Schlegel, G. E. Scuseria, M. A. Robb, J. R. Cheeseman, G. Scalmani, V. Barone, G. A. Petersson, H. Nakatsuji, X. Li, M. Caricato, A. V. Marenich, J. Bloino, B. G. Janesko, R. Gomperts, B. Mennucci, H. P. Hratchian, J. V. Ortiz, A. F. Izmaylov, J. L. Sonnenberg, D. Williams-Young, F. Ding, F. Lipparini, F. Egidi, J. Goings, B. Peng, A. Petrone, T. Henderson, D. Ranasinghe, V. G. Zakrzewski, J. Gao, N. Rega, G. Zheng, W. Liang, M. Hada, M. Ehara, K. Toyota, R. Fukuda, J. Hasegawa, M. Ishida, T. Nakajima, Y. Honda, O. Kitao, H. Nakai, T. Vreven, K. Throssell, J. A. Montgomery, Jr., J. E. Peralta, F. Ogliaro, M. J. Bearpark, J. J. Heyd, E. N. Brothers, K. N. Kudin, V. N. Staroverov, T. A. Keith, R. Kobayashi, J. Normand, K. Raghavachari, A. P. Rendell, J. C. Burant, S. S. Iyengar, J. Tomasi, M. Cossi, J. M. Millam, M. Klene, C. Adamo, R. Cammi, J. W. Ochterski, R. L. Martin, K. Morokuma, O. Farkas, J. B. Foresman and D. J. Fox, 2016.

2 A. Kokil, K. Yang and J. Kumar, 2012, DOI: 10.1002/polb.23103.

3 A. Pivrikas, N. S. Sariciftci, G. Juška and R. Österbacka, *Prog. Photovoltaics Res. Appl.*, 2007, **15**, 677–696.

4 A. Ghosh, S. K. Seth, A. Ghosh, P. Pattanayak, A. Mallick and P. Purkayastha, *Chem. - An Asian J.*, DOI:10.1002/asia.202100117.

5 K. Maiti, A. K. Mahapatra, A. Gangopadhyay, R. Maji, S. Mondal, S. S. Ali, S. Das, R. Sarkar, P. Datta and D. Mandal, *ACS Omega*, DOI:10.1021/acsomega.6b00288.

6 D. C. Santra, M. K. Bera, P. K. Sukul and S. Malik, *Chem. - A Eur. J.*, 2016, **22**, 2012–2019.

7 J. Hwang, P. Nagaraju, M. J. Cho and D. H. Choi, 2023, DOI: 10.1002/agt2.199.

8 M. Chuai, T. Yang and M. Zhang, *J. Mater. Chem. A*, DOI:10.1039/c8ta01388h.

9 S. Shao and L. Wang, 2020, DOI: 10.1002/agt2.4.